AD-A181 445 THIN-FILM OPTOELECTRONIC CIRCUITS RESEARCH PROGRAM(U) 1/1
HONEYWELL INC BLOOMINGTON MN PHYSICAL SCIENCES CENTER
S M ARNOLD APR 87 AFOSR-TR-87-0770 F49620-85-C-0050
UNCLASSIFIED F/G 9/5 NL

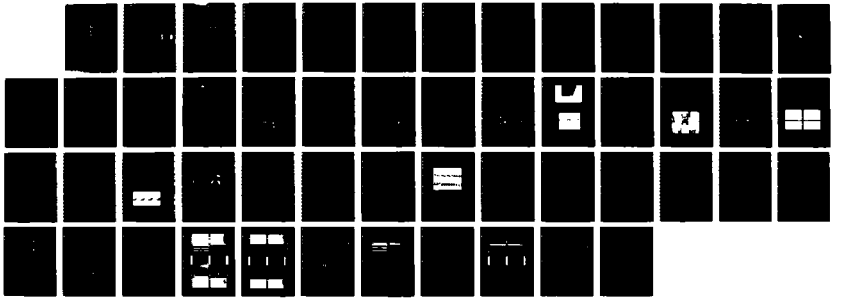

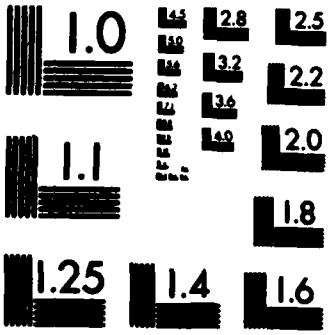

(2)

AFOSR-TR- 87-0770

THIN-FILM OPTOELECTRONIC CIRCUITS RESEARCH PROGRAM

Final Technical Report

AFOSR Contract No. F49620-85-C-0050

Submitted by:

Honeywell Physical Sciences Center
10701 Lyndale Avenue South
Bloomington, Minnesota 55420

April 1987

UNCLASSIFIED
SECURITY CLASSIFICATION

AD-A181445

REPORT DOCUMENTATION PAGE

1a REPORT SECURITY CLASSIFICATION: Unclassified	1b RESTRICTIVE MARKINGS
2a SECURITY CLASSIFICATION AUTHORITY	3 DISTRIBUTION / AVAILABILITY OF REPORT: Approved for public release: distribution unlimited
2b DECLASSIFICATION / DOWNGRADING SCHEDULE	
4 PERFORMING ORGANIZATION REPORT NUMBER(S)	5 MONITORING ORGANIZATION REPORT NUMBER(S): AFOSR-TR- 87-0770
6a NAME OF PERFORMING ORGANIZATION: Honeywell Inc. Physical Sciences Center; 6b OFFICE SYMBOL (If applicable)	7a NAME OF MONITORING ORGANIZATION: USAF, AFSC Air Force Office of Scientific Research
6c ADDRESS (City, State, and ZIP Code): 10701 Lyndale Avenue South Bloomington, MN 55420	7b ADDRESS (City, State, and ZIP Code): Bldg. 410 Bolling AFB, Washington, D.C. 20332
8a NAME OF FUNDING / SPONSORING ORGANIZATION: AFOSR; 8b OFFICE SYMBOL (If applicable): NE	9 PROCUREMENT INSTRUMENT IDENTIFICATION NUMBER: F49620-85-C-0050
8c ADDRESS (City, State, and ZIP Code): Bldg 410 BOLLING AFB DC 20332	10 SOURCE OF FUNDING NUMBERS: PROGRAM ELEMENT NO 61102F; PROJECT NO 2305; TASK NO B1; WORK UNIT ACCESSION NO

11 TITLE (Include Security Classification)
Thin-Film Optoelectronic Circuits Research Program (Unclassified)

12 PERSONAL AUTHOR(S)
Steven M. Arnold

13a TYPE OF REPORT	13b TIME COVERED	14 DATE OF REPORT (Year, Month, Day)	15 PAGE COUNT
Final Technical	FROM 85/2/1 TO 87/1/31		49

16 SUPPLEMENTARY NOTATION

17 COSATI CODES		
FIELD	GROUP	SUB-GROUP

18 SUBJECT TERMS (Continue on reverse if necessary and identify by block number)
Integrated Optics; Electro-Optic Devices; Gallium Arsenide (GaAs); Thin-Film Waveguides; Zinc Oxide (ZnO)

19 ABSTRACT (Continue on reverse if necessary and identify by block number)

The program objective has been to identify and investigate IC-compatible fabrication processes for thin-film optoelectronic circuits on GaAs. Single-mode channel waveguides of SiO_2-ZnO-SiO_2, SiO_2-Al_2O_3-Ta_2O_5-SiO_2, and SiO_2-Al_2O_3-SiO_2 have been deposited on GaAs by ion-beam sputtering. Straight guides, curves, tapers, Y-branches, crossovers, and directional couplers have all been demonstrated. Novel concepts have been developed for integrated GaAs Schottky photodiodes and self-aligning fiber-to-waveguide couplers. An IC-compatible baseline fabrication process has been established and a photomask set has been completed for an optoelectronic circuit demonstration, including Mach-Zehnder interferometric modulators, delta-beta electro-optic switches, and integrated GaAs photodetectors.

20 DISTRIBUTION / AVAILABILITY OF ABSTRACT	21 ABSTRACT SECURITY CLASSIFICATION
☐ UNCLASSIFIED/UNLIMITED ☒ SAME AS RPT ☐ DTIC USERS	Unclassified
22a NAME OF RESPONSIBLE INDIVIDUAL: Bles	22b TELEPHONE (Include Area Code): 202 767-4931; 22c OFFICE SYMBOL: NE

DD FORM 1473, 84 MAR — 83 APR edition may be used until exhausted. All other editions are obsolete.

SECURITY CLASSIFICATION OF THIS PAGE
Unclassified

THIN-FILM OPTOELECTRONIC CIRCUITS RESEARCH PROGRAM

Final Technical Report

AFOSR Contract No. F49620-85-C-0050

by

Steven M. Arnold

April 1987

Honeywell Physical Sciences Center
10701 Lyndale Avenue South
Bloomington, Minnesota 55420

Approved by: _____ Date: 5/6/87
Anis Husain, Section Head

_____ Date: 5/11/87
Dave Fulkerson, Department Manager

Table of Contents

Section		Page
I	INTRODUCTION	1-1
	Statement of the Problem	1-1
	Zinc Oxide on Gallium Arsenide	1-1
	Summary of Approach	1-3
II	TECHNICAL OBJECTIVES	2-1
	Long-Term Objective	2-1
	Objectives of the Research Program	2-1
III	RESULTS AND DISCUSSION	3-1
	Zinc Oxide Material	3-1
	Fabrication Process Overview	3-3
	Waveguide Structures	3-5
	Fiber-to-Waveguide Coupling	3-14
	Electro-Optic Switches and Modulators	3-18
	Integrated Photodetectors	3-19
	Summary of Accomplishments	3-22
IV	DIRECTIONS FOR FUTURE RESEARCH	4-1
V	APPENDIX	5-1
	Key Personnel	5-1
	Publications	5-1
	Acknowledgement	5-1
	Phase I Mask Set	5-2
	Phase II Fabrication Process	5-3
	Phase II Mask Set	5-6

List of Illustrations

Figure		Page
1-1	Thin-Film Waveguide Structure	1-3
1-2	Delta Beta Electro-Optic Switch	1-4
1-3	Mach-Zehnder Interferometric Switch	1-5
1-4	Fiber-to-Waveguide Coupling	1-6
1-5	Integrated Waveguide Photodetector	1-6
3-1	Modes of ZnO Thin-Film Waveguide	3-1
3-2	Measurement of Modal Indices	3-2
3-3	Measurement of Planar Waveguide Attenuation	3-2
3-4	Fabrication Process Overview	3-4
3-5	Channel Waveguide Fabrication Process	3-7
3-6	Chlorobenzene-Soaked Photoresist Shadow Mask	3-8
3-7	Two-Layer Photoresist Shadow Mask	3-8
3-8	Dependence of Ridge Height on Channel Width	3-9
3-9	End-Fire Coupling Facility	3-10
3-10	Channel Waveguide Mode Profiles	3-11
3-11	Photos of Channel Waveguide Mask	3-12
3-12	Propagation Loss of Single-Mode Channel Waveguides	3-14
3-13	Etched Vee-Grooves in GaAs	3-15
3-14	Etched Vee-Grooves in Silicon	3-16
3-15	Dependence of Mode Dimension on ZnO Film Thickness	3-17
3-16	Concept for Fiber-to-Waveguide Mode Matching	3-18
3-17	Integrated Schottky Photodetectors	3-20
3-18	I-V Characteristics of Integrated Photodetector	3-21
5-1	Program Organization	5-1
5-2	Computer Plot of Phase I Mask Set	5-2
5-3	Computer Plots of Phase II Mask Set	5-6

List of Tables

Table		Page
1-1	Electro-Optic Waveguide Materials	1-2

Section I
INTRODUCTION

STATEMENT OF THE PROBLEM

Monolithic integration of electronic circuits in silicon has made possible a revolution in electronic computation and signal processing. Today, gallium arsenide integrated circuits (GaAs ICs) are extending this electronic revolution to ever higher speed devices.

Optical signal processing, despite its consistent advances and several early successes such as synthetic aperture radar and the optical spectrum analyzer, is falling increasingly behind the electronic competition. Functions which formerly required the speed and parallelism of optics are now being implemented entirely in digital electronics. The reasons for this are several, but one in particular stands out: the lack of emphasis given to compatibility issues between optical and electronic IC fabrication processes. As a result, most integrated optic devices demonstrated to date have been discrete components requiring laborious interfacing to predominantly electronic systems.

For integrated optical signal processors to compete on a cost basis with digital electronics, monolithic optoelectronic integration will be required. Optical waveguides, switches, modulators, sources and detectors as well as electronics must be integrated on a single substrate. Microelectronics, being the dominant technology, will not likely bend to accommodate the optics. Therefore, integrated optics must seek better compatibility with mainstream microelectronics.

ZINC OXIDE ON GALLIUM ARSENIDE

Honeywell's approach to IC compatible optoelectronic integration uses thin-film waveguides of zinc oxide (ZnO) on substrates of gallium arsenide. Table 1-1 offers a comparison of thin-film ZnO with two more prevalent waveguide materials--lithium niobate ($LiNbO_3$) and aluminum gallium arsenide (AlGaAs).

$LiNbO_3$ is the current research material of choice for integrated optics. It is reasonably transparent and has strong electro-optic and piezo-electric properties. Channel waveguides are fabricated in $LiNbO_3$ by in-diffusion of titanium. The resulting waveguides have rather large mode dimensions which can be well matched to optical fibers. A number of researchers have demonstrated impressive integrated optic devices in $LiNbO_3$. The chief disadvantage of $LiNbO_3$ is that it offers no possibilities for monolithic integration of detectors, electronics, or light sources. Also, coupling of $LiNbO_3$ devices to other optical components requires expensive polishing and alignment operations.

Table 1-1. Electro-Optic Waveguide Materials

PROPERTY	MATERIAL		
	Thin Film ZnO	$LiNbO_3$	AlGaAs on GaAs
Fabrication Method	Sputtered film	Ti diffusion	Epitaxial growth
Refractive Index	2.0	2.2	3.5
Attenuation	> 0.1 dB/cm	> 0.5 dB/cm	4 to 40 dB/cm at 800-850 nm
Electro-Optic Coefficient (10^{-12} m/V)	r_{13} = -1.4 r_{33} = +2.6	r_{13} = +8.6 r_{33} = +30.8	r_{41} = -1.5
Piezoelectric Effect	Moderate	Strong	Very weak
Fiber Coupling Methods	Cleave & butt Si vee-grooves	Polish & butt	Cleave & butt
Mode Matching to Fiber	More difficult	Easy	More difficult
Electronics Compatible?	Yes	No	Yes, but...
Laser Compatible?	Yes, on GaAs	No	Yes
First Lab Demo	1969	1974	1970
3-inch Wafer Cost	$ 7	$ 200	$ 250

AlGaAs is often cited as a material system permitting full monolithic integration of high-speed microelectronics, optical waveguides, and diode lasers. Honeywell was the first to demonstrate the monolithic integration of an AlGaAs transverse junction stripe (TJS) laser with a GaAs 4:1 multiplexer. Such full optoelectronic integration is very difficult because the electronic properties of GaAs are degraded by the high temperature processes required for growing lasers and waveguides. Also, AlGaAs waveguides have rather high optical losses at AlGaAs laser wavelengths of 800-850 nm.

Deposited waveguides of ZnO or other thin-film materials have a number of advantages over either bulk crystal ($LiNbO_3$) or epitaxially grown (AlGaAs) waveguides. Thin films can be sputter deposited inexpensively on a variety of substrates including both Si and GaAs. The sputtering is done at relatively low temperatures, permitting the fabrication of microelectronics and/or lasers on the same substrate. Because of their lower optical loss and lower temperature of deposition, thin-film waveguides are an attractive alternative to AlGaAs waveguides for monolithic integration on GaAs.

Similarity of mode profiles and ease of alignment are important considerations when coupling integrated optical devices to optical fibers or diode lasers. Compared to $LiNbO_3$ waveguides, the mode profiles of thin-film waveguides are less well matched to those of

optical fibers but better matched to diode lasers. Precise vee-grooves can be anisotropically etched into substrates of Si, thus providing inexpensive alignment between thin-film waveguides and optical fibers.

Zinc oxide is unique among thin-film waveguide materials. Sputter deposited ZnO films are polycrystalline with the c-axis oriented normal to the substrate. ZnO has sizeable piezo-electric, electro-optic, and nonlinear optical coefficients, making it possible to fabricate surface acoustic wave (SAW) and active optical devices in the same film. Waveguides of ZnO can have very low optical losses, with values as low as 0.01 dB/cm having been reported for laser annealed planar films on oxidized silicon.

SUMMARY OF APPROACH

The following several paragraphs summarize the basic optical components --waveguides, switches, couplers, and detectors--required for fabricating thin-film ZnO on GaAs optoelectronic circuits.

The structure of our thin-film channel waveguides is depicted in Figure 1-1. Light is confined to the ZnO film which is sandwiched between two lower index layers of SiO_2. For single mode operation, the thickness of the ZnO layer is about 0.3 micron while the lower SiO_2 (buffer) layer must be 1.0 micron or more to minimize coupling to the higher index substrate. While waveguides on Si have generally used a thermally grown buffer layer, GaAs substrates necessarily require a deposited oxide. A second oxide layer, deposited over the ZnO, provides passivation and a symmetric mode structure.

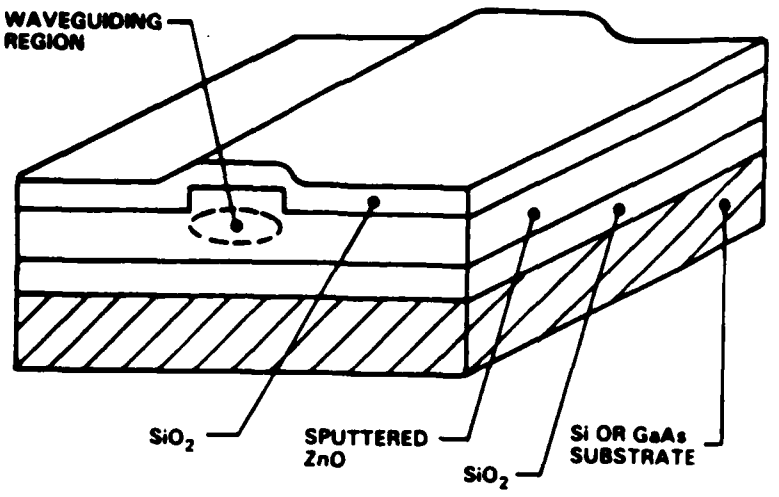

Figure 1-1. Thin-Film Waveguide Structure. Vertical confinement is provided by the planar SiO_2-ZnO-SiO_2 structure. Thicker ZnO in the channel region produces lateral confinement by locally increasing the effective refractive index.

Lateral confinement of the optical mode is provided by ridge structure which increases the effective refractive index in the channel region. Various combinations of ridge height and width will result in single mode waveguides, but a width of 2.5 microns and a height of about 100 Å provide a good compromise between ease of fabrication and acceptable bending losses. Since the ridge height is rather small, scattering due to sidewall roughness can be minimal.

An electro-optic switch of the 4-port directional coupler delta beta type is depicted in Figure 1-2. This type of switch can be readily fabricated in ZnO waveguides and is useful for crossbar networks and other applications in which light must be switched from one channel to another. The fraction of light coupled into the parallel guide is a periodic function of the interaction length. Generally, this length is chosen to be a bit longer than one half coupling period. A voltage across the electrodes produces equal and opposite refractive index changes (electro-optic effect) in the two guides. The resulting imbalance modifies the coupling. The split electrode configuration assures that the coupling can be electrically tuned between zero and 100 percent without the need for achieving exactly one half coupling period.

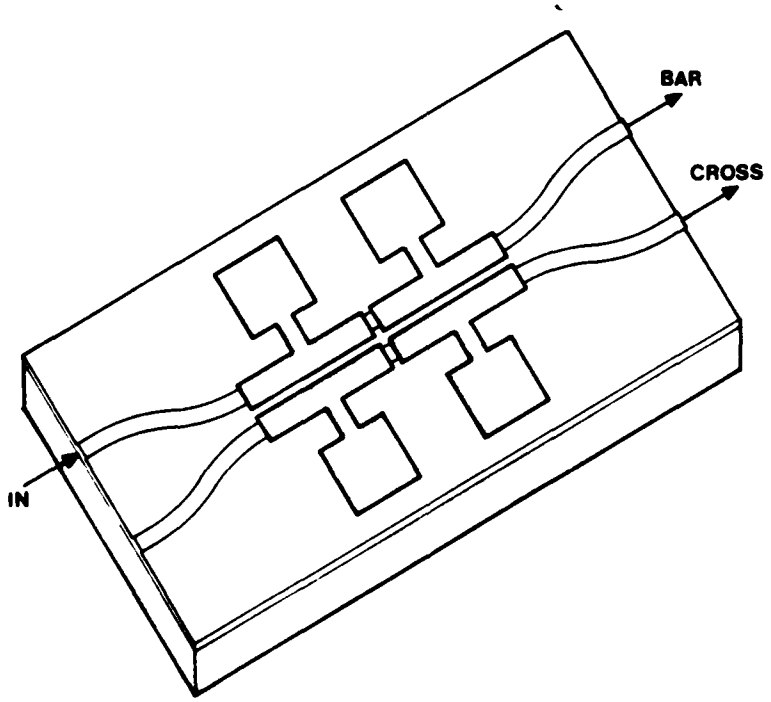

Figure 1-2. Delta Beta Electro-Optic Switch. Coupling between the two waveguides depends on their separation, length of interaction, and any differences in mode velocity (beta). Length and separation are chosen to give complete crossover. A voltage across the electrodes then unbalances the mode velocities to prevent crossover.

A second type of electro-optic switch, the Mach-Zehnder interferometer, is depicted in Figure 1-3. This is essentially an intensity modulator. A first Y-branch divides the light equally between the two legs of the interferometer. A second Y-branch then recombines the light following an electro-optic phase shift applied differentially between the two legs. The in-phase fraction of the light is coupled to the output guide while the out-of-phase portion is lost to radiation modes.

Figure 1-4 depicts the use of Si or GaAs vee-grooves for automatic alignment of optical fibers to thin-film waveguides. The vee-grooves, bounded by slow etching 111 crystallographic planes, are obtained by anisotropic etching. This approach is more production oriented than the lapping, polishing, and micropositioning technique currently required for attaching fibers to $LiNbO_3$ integrated circuits.

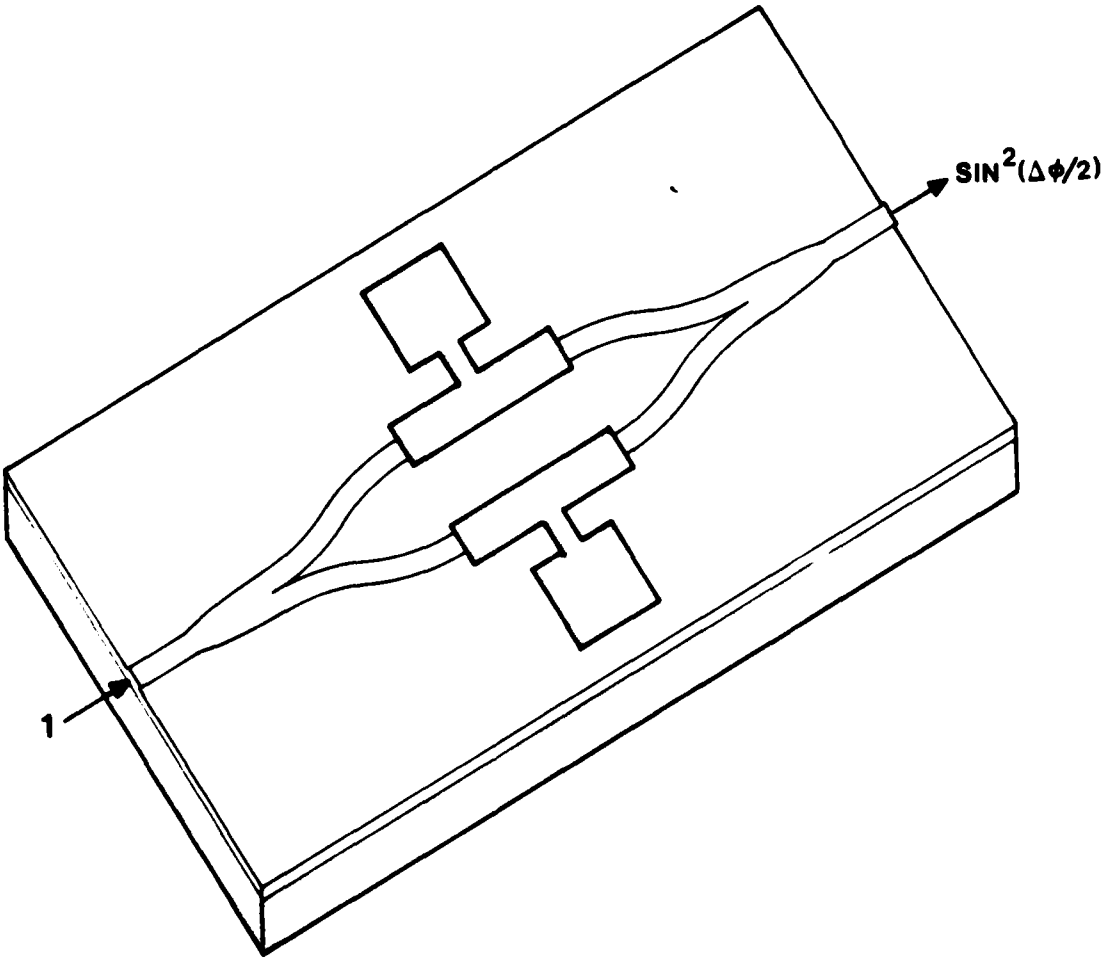

Figure 1-3. Mach-Zehnder Interferometric Switch. A voltage applied to the electrodes modulates the output channel. Since the output waveguide is single mode (no antisymmetric modes), any phase mismatched light is coupled to radiation modes.

One of the strengths of the thin-film ZnO on GaAs approach to optoelectronic circuits is that Schottky diode photodectors can be easily fabricated in the GaAs substrate. Figure 1-5 depicts how light may be coupled from a waveguide to such a detector. Waveguide-to-detector coupling occurs through an opening in the buffer layer. Optimal coupling would require tapering of the buffer layer to prevent the back reflections which result from an abrupt discontinuity.

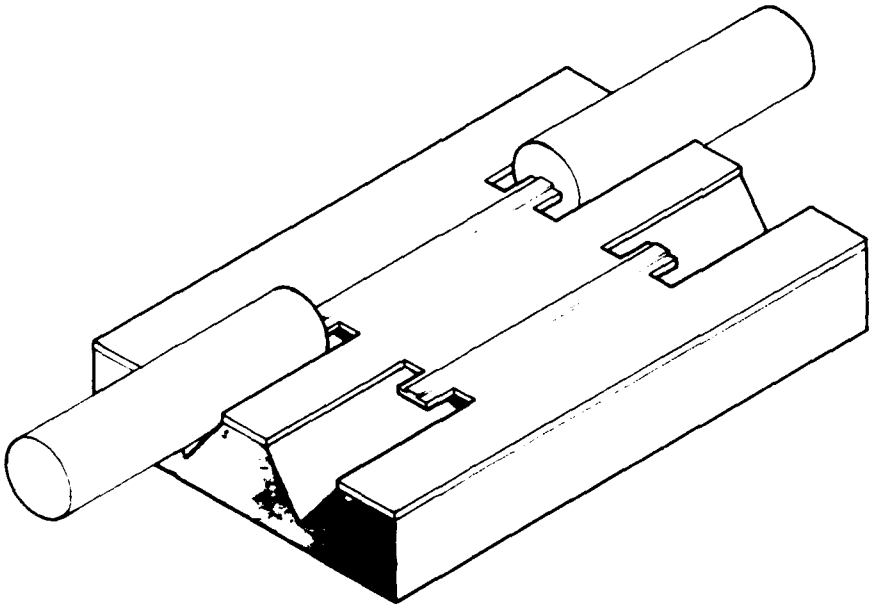

Figure 1-4. Fiber-to-Waveguide Coupling. Precision vee-grooves, anisotropically etched into the GaAs substrate, provide alignment of fibers to channel waveguides.

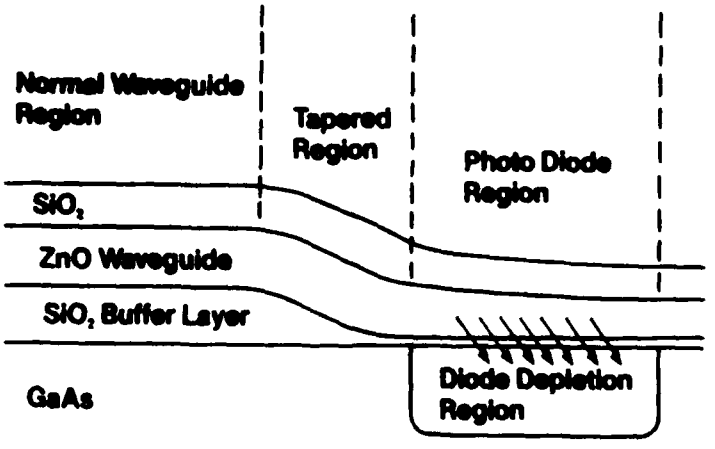

Figure 1-5. Integrated Waveguide Photodetector. An opening in the SiO_2 buffer layer causes light to be coupled to the high index GaAs substrate.

The foregoing discussion summarizes our approach to monolithic integration of waveguides, switches, couplers, and detectors on a GaAs substrate. The emphasis throughout is on compatibility with mainstream GaAs microelectronics fabrication processes. Although optically passive devices may be realized using fiber-to-chip or laser-to-chip interconnects, the more useful devices will ultimately require monolithic integration of AlGaAs lasers. While laser integration is beyond the scope of this program, it is our primary justification for selecting a GaAs substrate.

The following sections will review the objectives and accomplishments of the program and suggest possible directions for future research.

Section II
TECHNICAL OBJECTIVES

LONG-TERM OBJECTIVE

The long-term objective in pursuing this research program has been to develop monolithic optoelectronic circuits of thin-film zinc oxide on gallium arsenide (ZnO on GaAs) for optical signal processing applications.

Zinc oxide is a unique waveguide material in that it can be sputter deposited at low temperatures to form well-oriented polycrystalline films having very low optical losses and reasonably large piezoelectric and electrooptic effects. Deposited films of cadmium sulfide and aluminum nitride films have similar piezoelectric and electrooptic properties, but are not reported to have exhibited low optical loss.

OBJECTIVES OF THE RESEARCH PROGRAM

The objective of the Thin-Film Optoelectronic Circuits Research Program has been to identify and investigate IC-compatible fabrication processes for thin-film optoelectronic circuits of ZnO on GaAs. This technology will enable the monolithic integration of optical components with mainstream GaAs and Si microelectronics.

Originally proposed as a three-year effort, the program was later condensed to two years at the request of the sponsor.

During the first year of the program, we successfully met our objective of identifying and demonstrating IC-compatible fabrication methods for discrete optical components including waveguides, switches, detectors, and fiber-to-waveguide couplers.

During this second, final year of the program, we have largely met our primary objective of integrating most of these various optical components into optical circuits on GaAs while still maintaining IC process compatibility. As a demonstration vehicle, we attempted to fabricate 2 x 2 and 1 x 4 optical crossbar switches with fiber optic inputs and outputs. This demonstration was not completed because we were unable to obtain ZnO films of sufficient quality.

Section III
RESULTS AND DISCUSSION

This section reports our efforts to develop an IC-compatible fabrication processes for thin-film optical circuits on GaAs. Circuit components include channel waveguide structures, fiber-to-waveguide couplers, electro-optic switches, and integrated photodetectors. The section concludes with a summary of our accomplishments.

ZINC OXIDE MATERIAL

Figure 3-1 shows the theoretical dispersion curves of an SiO_2:ZnO:SiO_2 planar waveguide. ZnO film thicknesses near 3000 A yield single-mode guides with a maximum degree of confinement. Similar curves can be generated for waveguides lacking an upper passivation layer of SiO_2. Films were characterized prior to passivation by measuring their modal indices (N_{eff}) and waveguide attenuation. Modal indices were converted to ZnO film thickness and refractive index by fitting to the theoretical dispersion curves. The measurement techniques, utilizing rutile prisms, are depicted in Figures 3-2 and 3-3.

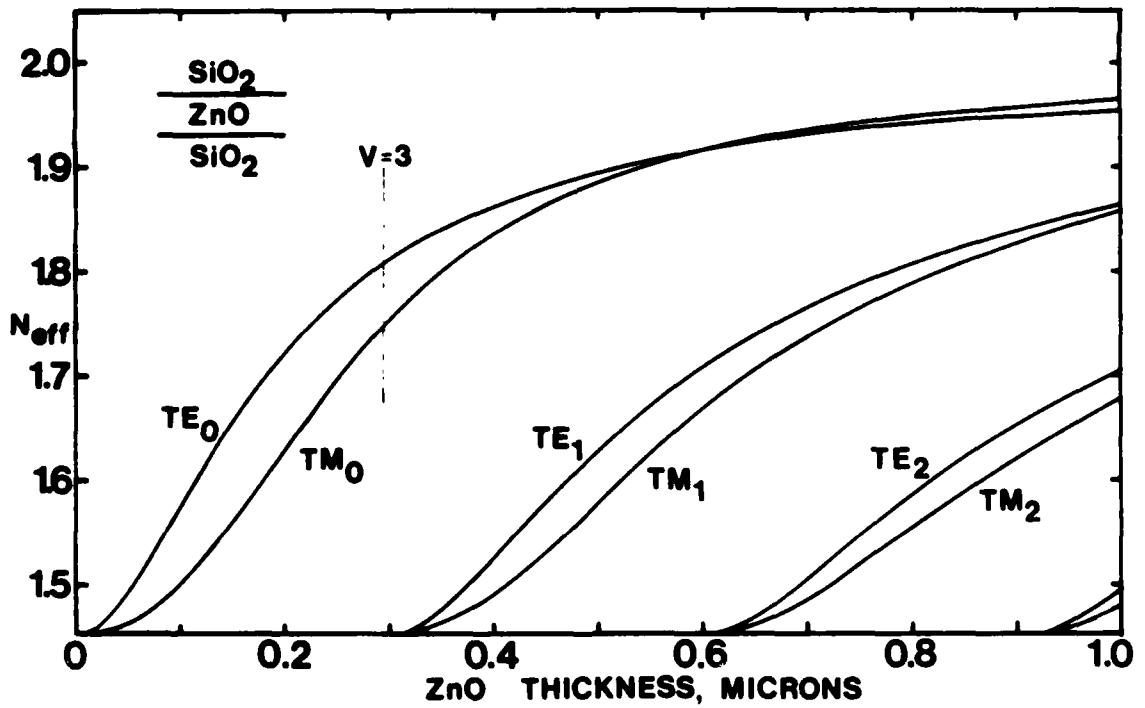

Figure 3-1. Modes of ZnO Thin-Film Waveguide. Single mode operation is achieved with a ZnO film thickness near 3000 A.

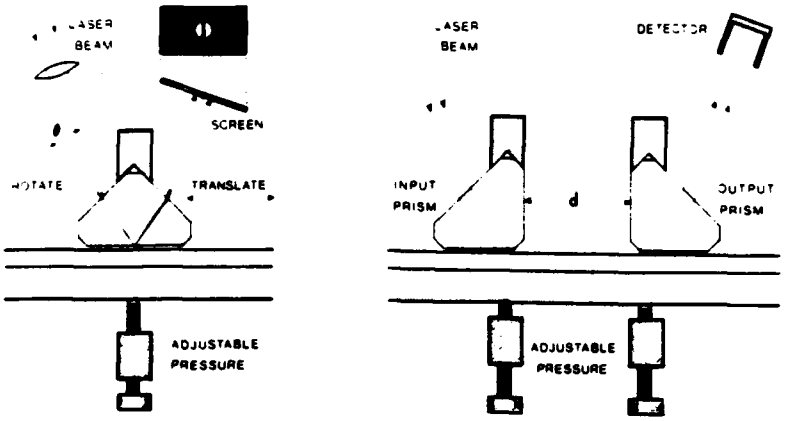

Figure 3-2. Measurement of Modal Indices. The assembly is rotated until the reflected beam is bisected by a dark line, the missing light being coupled to a waveguide mode. Modal indices are computed from the measured coupling angles.

Figure 3-3. Measurement of Planar Waveguide Attenuation. The output prism is repeatedly removed and replaced closer to the input prism. Attenuation (dB/cm) is obtained from a plot of optical throughput (dB) versus prism separation (cm).

From the beginning, our efforts were hampered by difficulties in depositing ZnO films of suitable quality. This was primarily due to the vertical geometry of our RF sputtering system which gave a nonuniform film thickness and allowed "crumbs" of ZnO to rain down from the shutter and onto the substrate. The "crumb" problem was temporarily resolved at considerable effort by a thorough cleaning of the apparatus, but the situation was less than satisfactory.

Because both this program and Honeywell's IR&D Fiber Optic Gyro program required high quality ZnO films, we elected to undertake an internally funded effort to develop ion beam sputtered ZnO films. We had previously demonstrated that ion beam sputtering could produce high optical quality SiO_2, TiO_2 and Al_2O_3 films, but we had not used this technique for the deposition of ZnO. While working to develop a ZnO material capability in collaboration with our Systems and Research Center, we have substituted films of non-electrooptic Al_2O_3 for ZnO in many of our devices. These high quality, ion beam sputter deposited Al_2O_3 films have permitted us to successfully demonstrate a number of thin film waveguide components. Any demonstration of electro-optic switches has, however, been unavoidably delayed.

In early 1986, our Systems and Research Center began been depositing waveguiding films of ion beam sputtered ZnO. These films are well-oriented and of uniform thickness and quality over a 3-inch substrate. However, they are also quite conductive and have generally exhibited attenuation losses in excess of 25 dB/cm. We suspect that their poor optical and electrical properties are attributable to incomplete oxidation. While further development effort may improve the quality of ion beam sputter deposited ZnO films, they were of little use to the Thin-Film Optoelectronic Circuits Program.

When it became clear that Honeywell's ZnO materials capability would not meet the needs of the Thin-Film Optoelectronic Circuits Program, we began to investigate alternative sources. Encouraging initial discussions with the University of Arizona's Optical Sciences Center were soon hampered by the graduation and departure of a key student. After learning that APA Optics, a local firm, had deposited ZnO waveguides on glass substrates, we asked them to deposit ZnO films on five of our GaAs wafers. The optical quality of the APA Optics RF sputter deposited films, at 20-25 dB/cm, was little better than that of our System and Research Center's ion beam sputter deposited films.

Although we were not successful in obtaining optical quality ZnO films for the Thin-Film Optoelectronic Circuits Program, we did succeed in demonstrating a number of passive components, and we remain convinced of the merits of a thin-film approach to optoelectronic integration.

FABRICATION PROCESS OVERVIEW

Our optoelectronic circuit fabrication process is summarized in Figure 3-4 and described in the following paragraphs. The earliest version of this process served as a framework for the design and layout of the Phase II optical circuit demonstration mask set. The process has since been considerably refined based on actual device fabrication experience. The Phase II mask set and a sample run sheet giving details of the fabrication process are included in the Appendix (i.e. Section V).

The optical circuits fabricated by this process have an electro-optically active GaAs-SiO_2-ZnO-SiO_2 waveguiding structure with electrodes above and below the waveguiding film. The GaAs substrate includes Schottky photodiodes and was initially intended to have anisotropically etched vee-grooves for the alignment of optical fibers. In keeping with the program objectives, the process is fully compatible with mainstream GaAs IC fabrication and can potentially accommodate a large variety of active electro-optic and acousto-optic devices.

The fabrication process begins with the plasma deposition of an SiO_2 buffer layer to isolate the optical guided modes and switch electrodes from the semi-insulating and optically lossy GaAs substrate. If GaAs Schottky photodiodes are to be used, slots are then etched through this buffer layer to allow coupling between waveguides and detectors. Next, a first metallization layer is patterned to form the Schottky contacts, shunting electrodes for the electro-optic and acousto-optic devices, and

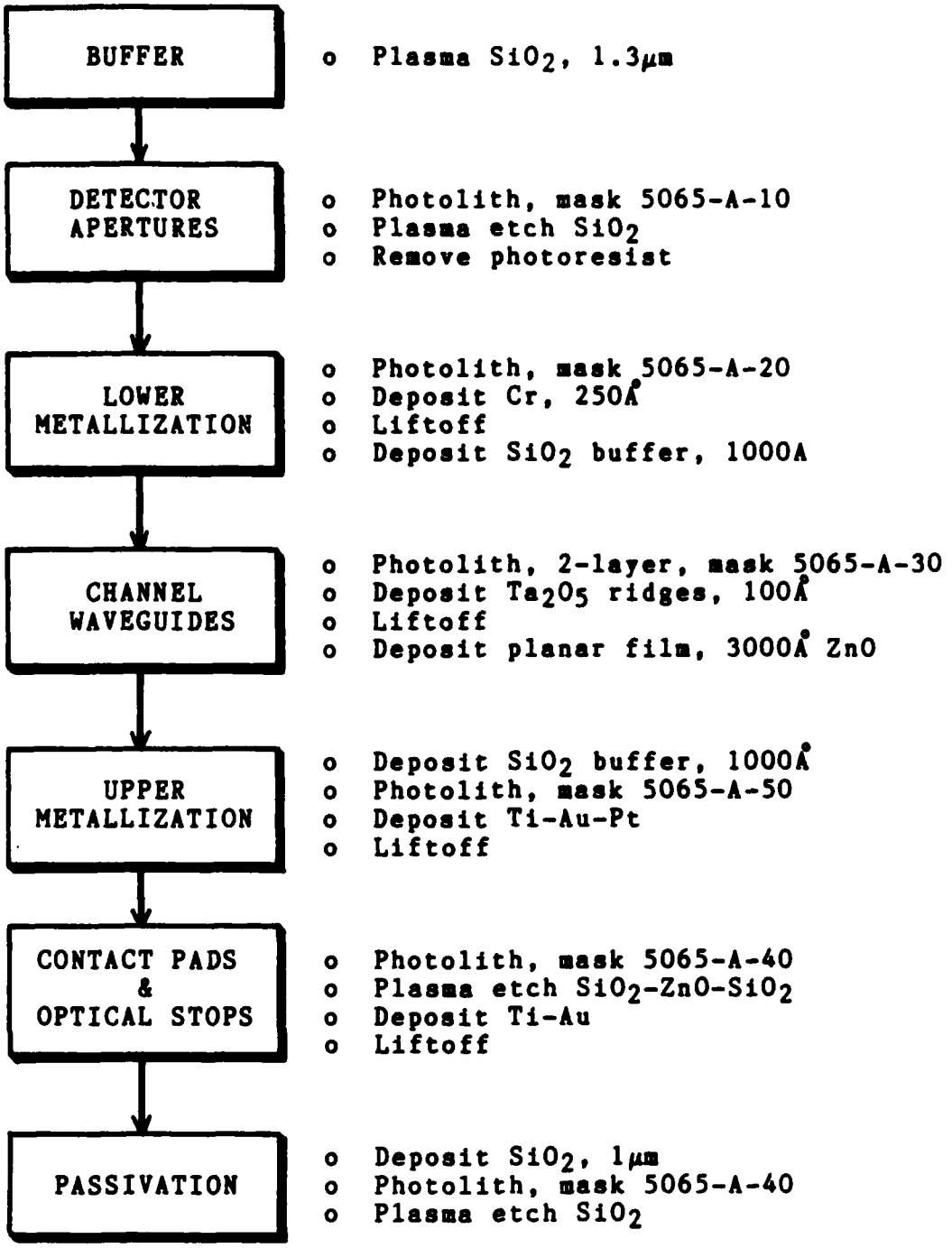

Figure 3-4. Fabrication Process Overview. This process is fully compatible with mainstream GaAs IC fabrication and can potentially accommodate a large variety of active electro-optic and acousto-optic devices.

also various alignment and identification marks. Since waveguides must pass directly over this first metallization (e.g., electro-optic switches), a second SiO_2 buffer layer is deposited to prevent optical attenuation by the metal electrodes (while still allowing efficient waveguide-to-detector coupling). In retrospect, the quality of the Schottky contacts could be improved by depositing them directly on the GaAs prior to any buffer layers, although the shunting electrodes, which are on the same mask, likely benefit by being electrically isolated from the substrate. The solution is to incorporate additional lithography and metallization steps specifically to define the shunting electrodes.

After the bottom electrode and buffer layer structures, the next step in the fabrication process is deposition of the ZnO channel waveguides using the two-step ridge and planar depositions as described previously. This is followed by another SiO_2 buffer layer, the upper electrode metallization, and a thicker SiO_2 passivation layer.

Electrical contacts to the device are established by etching through the oxide layers to the underlying bonding pads and then depositing additional gold by a liftoff process. During the same operation, optical stops are etched through selected portions of the SiO_2-ZnO-SiO_2 structure to prevent unwanted planar waveguide modes.

WAVEGUIDE STRUCTURES

One of the first problems to be resolved was the identification of a suitable buffer layer for isolating the optical guided wave from the lossy and higher index GaAs substrate. Adequate optical isolation requires a buffer layer thickness of about 1 micron. Sputtered oxides were unattractive because of their low deposition rates. In our previous work, we had used thermally oxidized silicon substrates. This gave a high quality buffer layer but required several hours in a high temperature furnace, thereby violating our goal of compatibility with microelectronics. Thermal SiO_2 served as a convenient standard of buffer layer quality, but it was of course not an option either for the upper passivation layer or with GaAs substrates.

We conducted a series of experiments to assess the relative merits of thermal, ion beam sputtered, and plasma deposited SiO_2 buffer layers. Plasma SiO_2 is attractive in that it can be deposited to considerable thicknesses quite rapidly. We deposited (or grew) 2 micron thick SiO_2 layers of each type on Si substrates. We then broke the wafers in half and deposited identical 1 micron thick Al_2O_3 waveguiding films on each of the halves to be directly compared (two dissimilar halves per deposition). We then measured propagation loss of the TE_0 mode for each sample using a pair of rutile prisms (Figure 3-3). To the ~0.5 dB/cm accuracy of the measurements, we observed no significant dependence of propagation loss on type of buffer layer. Since our fabrication process would involve no high temperature processing, we assumed that this result would be equally valid on GaAs substrates despite their higher temperature coefficient of expansion. We therefore adopted plasma SiO_2 as both buffer and passivation layer for subsequent work.

Following the identification of plasma SiO_2 as a suitable buffer layer, our second major goal was to develop a process for fabricating channel waveguide ridge structures. A general deficiency of channel waveguides is some degree of excess scatter due to side wall roughness. Our ridge waveguide structure has some inherent advantages in this respect. Since the ridge height is only 100-300 A and the optical mode is confined predominantly beneath the ridge, scattering from the ridge sidewalls should be much reduced. Our work prior to the program start had shown that a ridge of photolithographically deposited PMMA introduced little excess scatter. However, PMMA is quite hygroscopic and a suitable lower index material for a passivation layer would be difficult to find. We therefore decided to form the ridge using a high index material, preferably the same material as the waveguiding film (ZnO).

Our baseline approach to ridge waveguide fabrication required partial etching of the ZnO film everywhere except the ridge. It was a dismal failure. While virtually any etchant would attack the ZnO, our films were not uniform in their etch resistance, having both hard and soft features on a fine scale. This was likely related to grain or column structure in these oriented polycrystalline films. Consequently, both the ridge sidewalls and the surrounding planar film were left in a very rough condition producing unacceptably high scatter.

Our revised approach was to deposit the ridge in a separate operation using a liftoff process. We initially used either Si_3N_4 or Al_2O_3 for the ridge because these materials were more readily available than ZnO, and the ridge was thin enough compared to the underlying ZnO film that a different ridge material was not expected to significantly perturb the electrooptic or piezoelectric properties of the overall structure. We found that some tearing of the ridge occured during liftoff, giving a rather ragged sidewall in places.

Two further refinements brought us to our current fabrication process, depicted in Figure 3-5. First, a chlorobenzene soak was adopted to produce the overhanging photoresist structure shown in Figure 3-6. Following exposure, a 10 to 20 minute soak in chlorobenzene hardened the AZ-1350 photoresist to a depth dependent on the soaking time. During development, the deeper lying photoresist then dissolved at a faster rate than near the surface, causing the observed undercutting. The overhanging photoresist then acted as a shadow mask for the subsequent ZnO ridge deposition, eliminating any tearing during liftoff. As an added benefit, the ridge sidewalls were more rounded perhaps, although this would be difficult to confirm. The chlorobenzene soak was later replaced by a more dependable two-layer resist process in which the top layer of AZ-1350 was exposed and developed to serve as a mask for deep UV flood lamp exposure of the underlying layer of PMMA. The superior performance of the two-layer process is shown in Figure 3-7.

A final process refinement involves depositing the ridge prior to the planar film. This provides an opportunity for any residual roughness of the ridge sidewalls to be somewhat smoothed over during the subsequent planar deposition. Two additional benefits are that the more critical

deposition occurs earlier in the process and that ridge height may be adjusted to compensate for photolithographic variations in channel width while affording a later opportunity to control the overall (ridge plus planar) thickness.

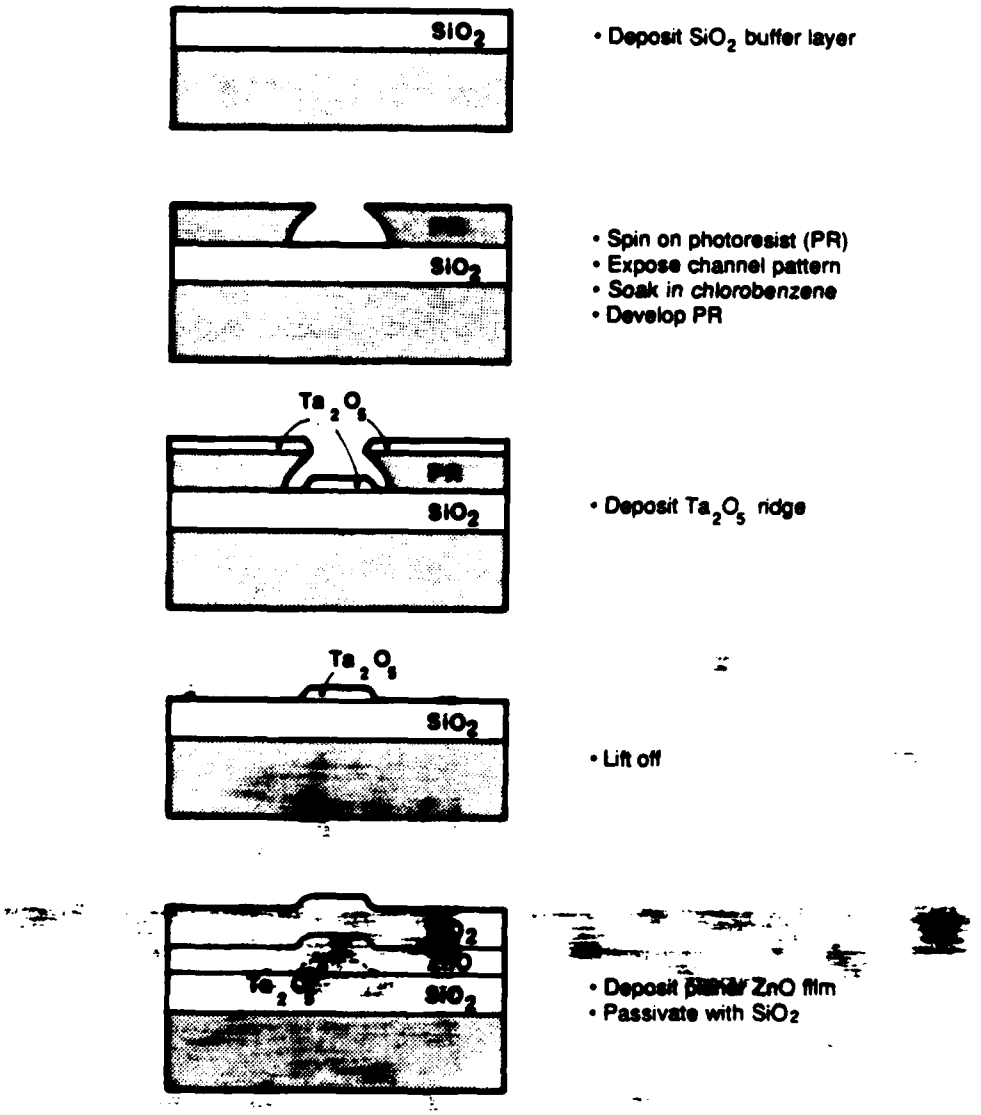

Figure 3-5. Channel Waveguide Fabrication Process. The overhanging photoresist shadow mask results in very smooth edges for the Ta_2O_5 ridge. These edges are perhaps further smoothed by the planar ZnO deposition.

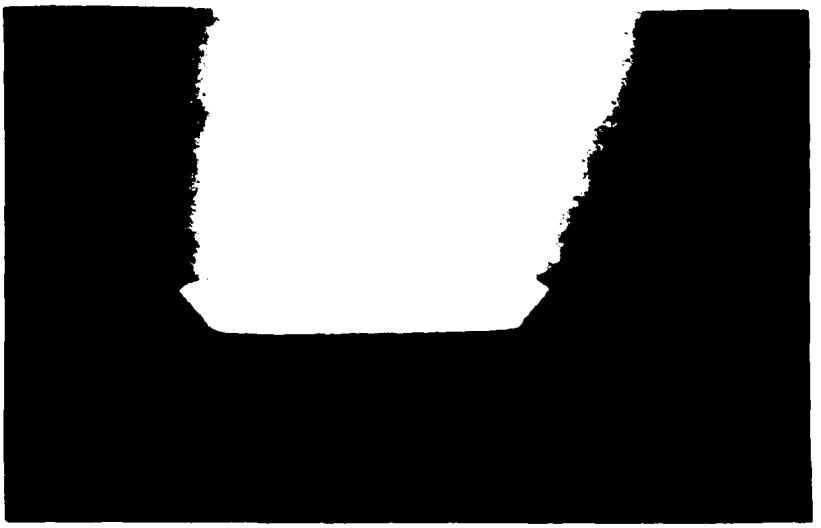

Figure 3-6. **Chlorobenzene-Soaked Photoresist Shadow Mask.** The overhang is adequate for liftoff but ridge deposition onto the "foot" yields rough sidewalls. The channel width is 3 microns.

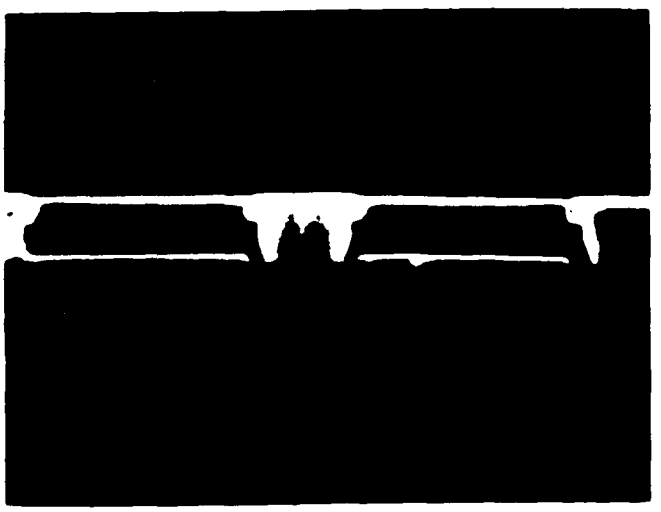

Figure 3-7. **Two-Layer Photoresist Shadow Mask.** The superior undercutting properties result in exceptionally smooth-walled waveguide ridges. Here, a metal has been deposited to better illustrate the process.

The tradeoff between ridge height and channel width is apparent in Figure 3-8 which shows the various combinations which yield single mode guides of optimal confinement (i.e. V = 3). Curves are shown for waveguiding films of ZnO and Al_2O_3 at wavelengths of 8300 A (AlGaAs) and 6328 A (He-Ne), in all cases with buffer and passivation layers of SiO_2. Thus, with a fixed channel width on the photomask, variation of ridge height was used to compensate for all changes in wavelength, materials, and processing.

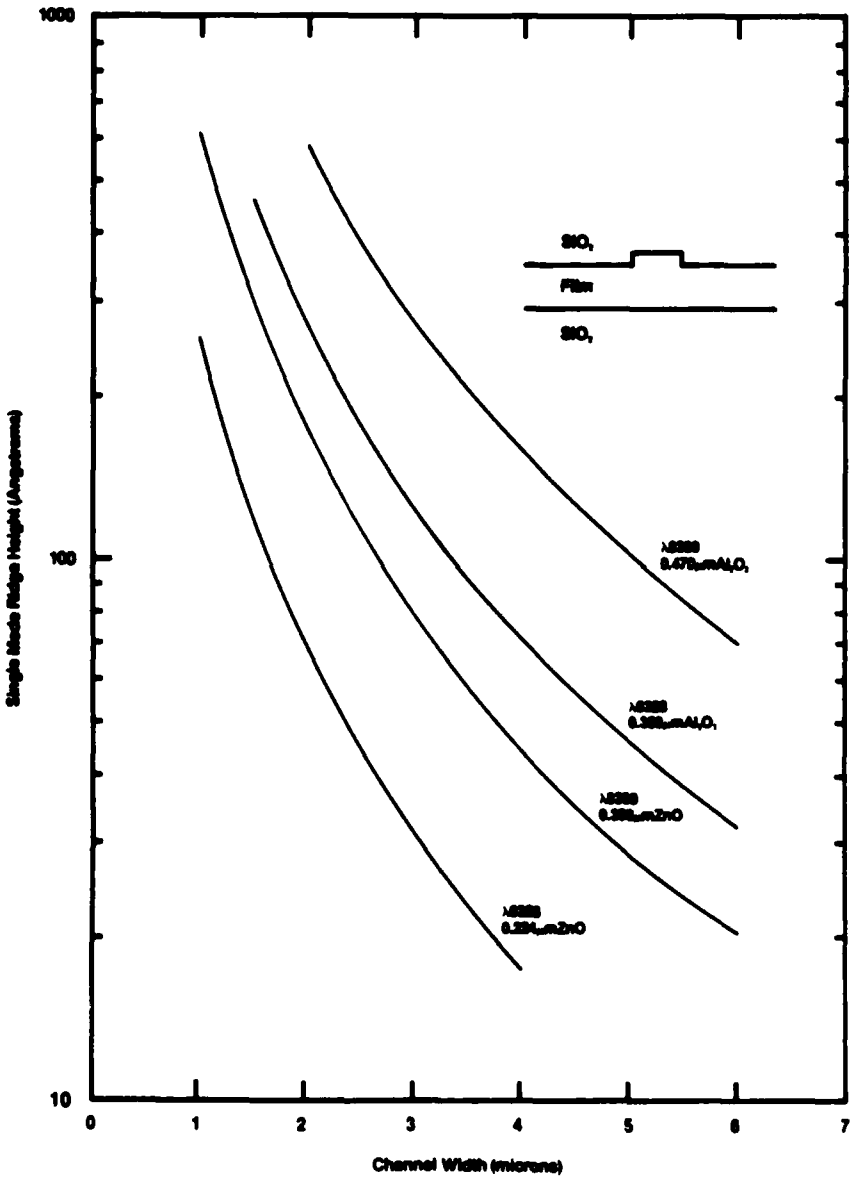

Figure 3-8. Dependence of Ridge Height on Channel Width. The curves are based on an effective index model.

The theoretically based curves of Figure 3-8 are based on an effective index approximation: separate three-layer planar waveguide solutions were obtained for the ridge and for the surrounding field, and the resulting modal indices were then used in solving an imaginary three-layer symmetric planar structure representing the waveguide in the lateral dimension. While this modeling technique is somewhat lacking in rigor, it is known to yield reasonable solutions so long as the ridge height is moderate and the mode is well confined. Numerical techniques would be required to obtain exact solutions.

The photomasks used in Phase I of the program were designed with waveguide channel widths of 2.5 microns. This seemed a reasonable compromise between adequate lateral confinement and ease of fabrication. However, in fabricating these channel waveguides, we found that the channel width often increased to 2.7 or 2.8 microns as a result of the various processing operations. It therefore became standard practice to measure channel width in the developed photoresist prior to depositing the waveguide ridges. This enabled us to adjust ridge height as a means of compensating variations in channel width. While the indicated ridge heights of only 150 to 300 A appeared to provide satisfactory lateral confinement for Al_2O_3 channel waveguides, we were not quite comfortable accepting ridge heights of 40 to 100 A for ZnO guides. Therefore, in designing a new mask set for Phase II of the program, we decreased the channel width to 2.0 microns. This resulted in actual device channel widths close to our target of 2.5 microns.

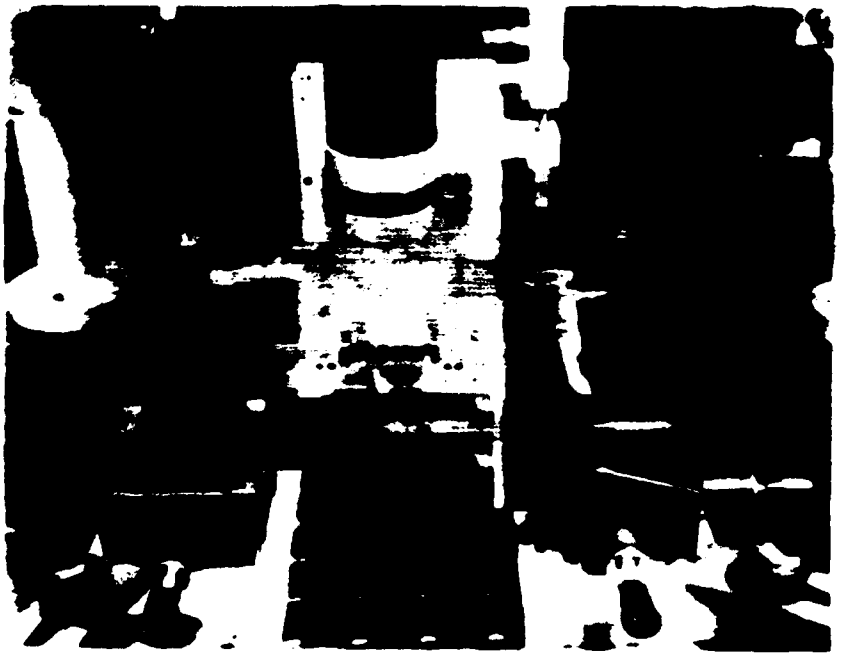

Figure 3-9. End-Fire Coupling Facility.

Channel waveguide devices were tested using the evaluation facility pictured in Figure 3-9. Polarized light from an AlGaAs diode laser (830 nm) was end-fire coupled into each sample using a diffraction limited 0.276 N.A. lens of 14.5 mm focal length. The output end of the waveguide was reimaged, 92 percent to a detector and 8 percent to a CID camera, by a somewhat faster 0.5 N.A. lens of 8.0 mm focal length. The frame-store equipped, 512 x 512 format, CID camera's 15 um x 15 um pixels scaled to 0.075 um x 0.075 um at the waveguide. The sample holder and lenses were each mounted on 3-axis translation stages, the sample's stage being equipped with piezo-translators providing 50 um of fine adjustment. The SMA-connectorized sample holder was designed for high speed electro-optical testing of appropriately packaged waveguide devices.

Figure 3-10 shows the near field TE and TM mode patterns of a typical channel waveguide. These digitized patterns have been renormalized to compensate for the frame-store board's AGC circuitry. The waveguides appear to be strictly single mode with no multiplicity of lobes and no apparent dependence of the profiles on input alignment. The observed mode dimensions, measured at the 1/e points, are 2.6 um x 1.3 um for the TE mode and 2.6 um x 1.2 um for the TM mode.

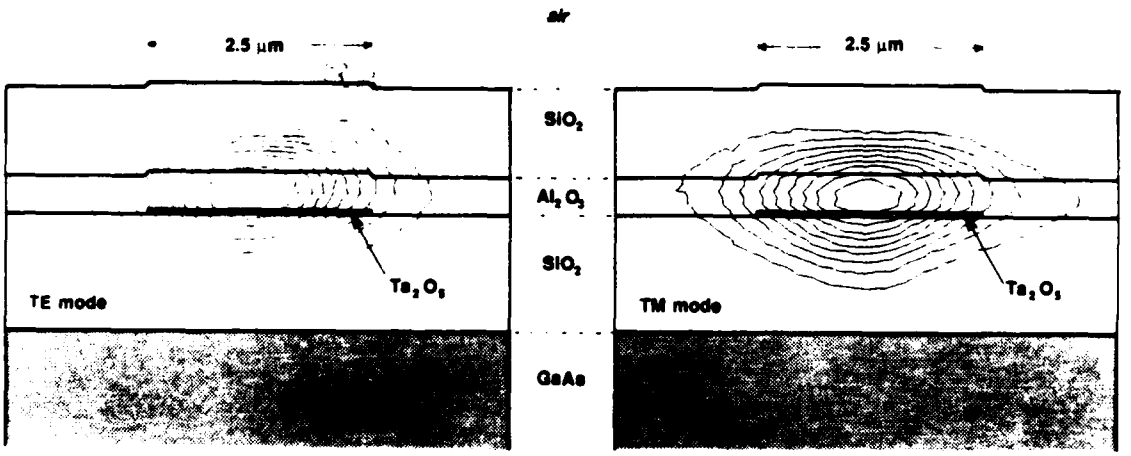

Figure 3-10. Channel Waveguide Mode Profiles. These near-field patterns were imaged to a CID camera. The contours represent 10 percent intensity intervals after background subtraction.

The presumed waveguide structure has been superimposed on the Figure 3-10 mode profiles. This structure consists of a 0.43 um thick Al_2O_3 film deposited over a 2.5 micron wide by 100 A thick ridge of Ta_2O_5. Ta_2O_5 was substituted as a ridge material because it has a refractive index similar to that of ZnO, which was not then available. Previous experience had shown our unannealed Ta_2O_5 to be quite lossy, but we

anticipated that in such a thin layer, it would have negligible effect on either the attenuation or the electro-optic properties of the result ing waveguide. Note that the Ta_2O_5 ridge thickness is not drawn to scale. When ZnO continued to be unavailable, we substituted the planar film of Al_2O_3. While correctly predicting single mode behaviour, the effective index model does not adequately describe the observed mode shape, predicting instead mode dimensions of 0.9 um x 4.6 um for the TE mode. Compared to the model predictions, the observed mode shapes are much better suited for coupling to optical fibers.

Figure 3-11 shows representative photos of the Phase I channel waveguide mask. Waveguide structures in the Phase II mask are similar. Mask photos are shown because the actual waveguides are nearly invisible and cannot be photographed. The Y-branch couplers consist of a parabolic tapered region which doubles the guide width, followed by a bifurcation region consisting of circular arcs. All curved waveguides were formed using circular arcs of maximum possible radius in order to minimize bending losses. The 4-port directional couplers consist of identical parallel waveguides plus curved sections to handle the offsets at each end. Coupling regions were 1 to 4 mm long with channel separations of 2 to 5 microns. Back-to-back tapers were included to assess the losses due to tapering. Design parameters of the Y-branches, directional couplers, and tapers were based on established mathematical models.

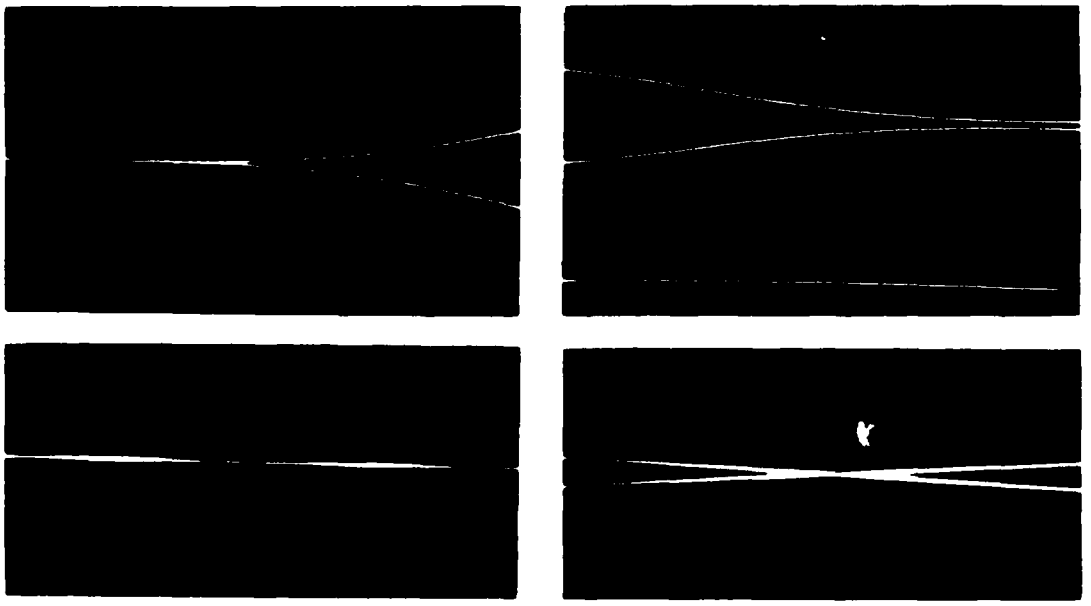

Figure 3-11. Photos of Channel Waveguide Mask. A Y-branch coupler, part of a directional coupler, back-to-back tapers, and a crossed channel structure are pictured.

We originally proposed crossed channel waveguides as a means of implementing electro-optic grating switches in channel waveguides. Later design analysis showed that a sufficiently long interaction length (crossing region) could not likely be obtained. Nonetheless, such structures are of some interest for the routing of signals, and we therefore continued to occasionally measure the insertion loss and crosstalk properties of these structures.

Key design parameters of a crossed channel waveguide are the guide width in the crossing region and the angle of intersection. Parabolic tapers were used to expand the crossed channels to widths varying from 2.5 um (no taper) to 30 um. The wider guides are therefore multimode in the crossing region, although all light is intended to remain only in the lowest order mode. Wider tapers were expected to yield lower crosstalk at the expense of greater mode conversion loss. The angle of intersection of Phase I crossed channel waveguides varied from 1.5 to 3.0 degrees with the shallower angles resulting in unacceptable crosstalk. All crossed channels on the Phase II mask set intersected at 3.0 degrees.

We used end-fire techniques to couple 830 nm laser light into various SiO_2-Al_2O_3-SiO_2-GaAs channel waveguide structures and then measured the output intensity at each associated output port. Comparing the total output intensity of each complex structure with that of a simple straight channel guide, we were able to deduce the insertion loss of each device. Similarly, by comparing the ratios of output intensities from the multiple ports of a single device, we were able to determine such quantities as branching ratios and crosstalk.

The overall conclusion from our measurements on complex waveguide structures--tapers, Y-branches, or crossovers--was that none of them appeared to introduce appreciable insertion loss. Each sample had some bad ports, perhaps as a result of point defects, but no single structure yielded consistently low throughput from sample to sample. Similarly, the Y-branch structures appeared to divide the optical power evenly between their branches, showing no more variation between their output ports than typical pairs of adjacent straight guides. Concerning the crossed channel waveguide structures, it was observed that those with no expansion (2.5 um width) or minimal expansion (5.0 um width) exhibited significant crosstalk. However, even the widest (30 um) crossed channels showed no significant insertion losses attributable to their tapers.

When we had finished the throughput measurements of the more complex waveguide structures on a sample, we then occasionally used a destructive cutback method to determine the propagation losses of the straight channel waveguides. Samples were always shortened from the output end in order to maintain constant input coupling. Figure 3-12 shows the results of one such series of measurements. The data for four parallel straight channels show an average propagation loss of less than 1.0 dB/cm. The anomalous data points for the 0.7 cm sample length result from an obviously bad edge cleave.

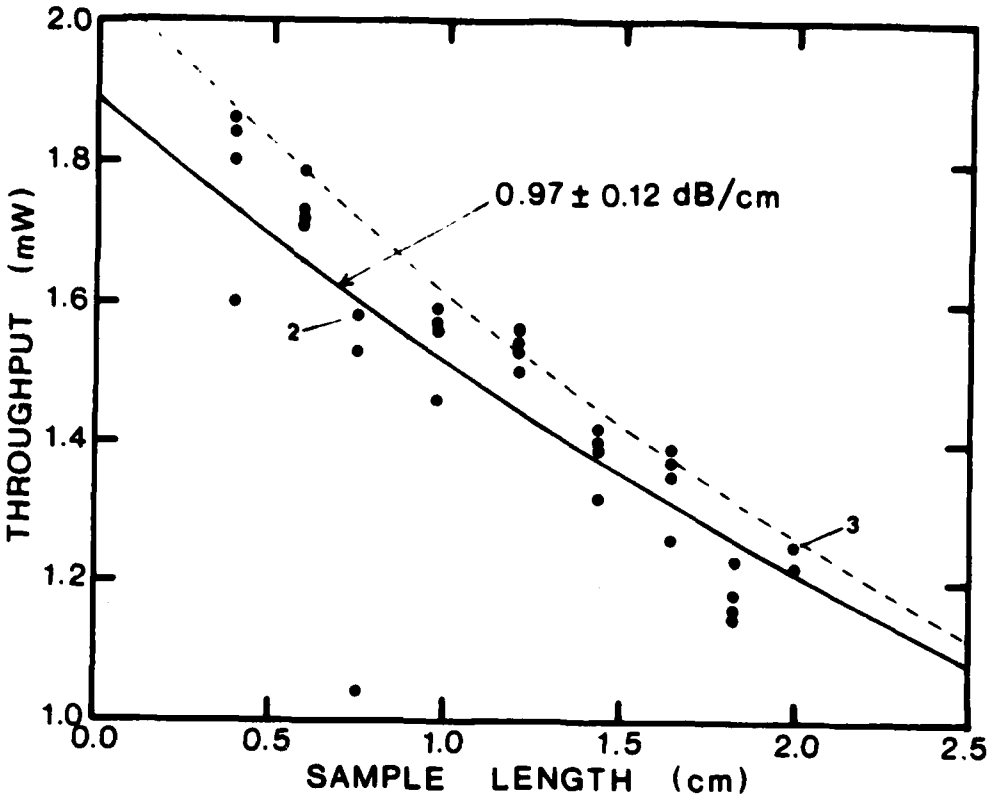

Figure 3-12. Propagation Loss of Single-Mode Channel Waveguides.

FIBER-TO-WAVEGUIDE COUPLING

Initially, fiber-to-fiber coupling tests were used to determine the suitability of etched vee-grooves for fiber alignment. Single-mode fibers having a 125 micron cladding diameter and a 5 micron core diameter were butt-coupled using silicon vee-grooves for alignment. Coupling efficiencies of 80 percent and better were routinely obtained. Coupling efficiency showed little dependence on axial rotation, indicating that concentricity of fiber core and cladding would not be a significant problem.

We found that fiber-to-fiber vee-groove splices could be made permanent by cementing with UV curing epoxy. As a side benefit, the index matching properties of the epoxy led to improved coupling efficiency. To solve a problem of excess epoxy contaminating adjacent vee-grooves, a technique was developed whereby the cleaved fiber end was dipped in epoxy and then wiped almost clean prior to insertion in the vee-groove. We found that the slight pressure required to seat an epoxied fiber in a vee-groove could be varied somewhat to fine tune the coupling. This provided a means of compensating variations in fiber diameter and groove depth.

Our proposed approach to fabricating the fiber-to-waveguide coupler of Figure 1-4 involved opening channels in the deposited SiO_2-ZnO-SiO_2 waveguide structure and using the oxide layers as an etch mask for the anisotropic vee-groove etch. Because of the difficulty of doing photo lithography on significantly nonplanar substrates, this vee-groove etch should be the final step in the fabrication process. A LAM (plasma) etcher was used for making quite vertical cuts through the oxides, stopping at the GaAs substrate.

Ideally, the depth of vee-grooves would be limited by the boundaries of the LAM-etched slots in the oxide and by 111 crystallographic planes of the GaAs substrate. To align the core of a 125 micron diameter fiber to a thin-film waveguide requires a groove width of 150 to 152 microns. A longer etching time should produce a deeper but not a wider vee-groove. Silicon etchants approach this ideal and the precision with which vee-grooves can be etched into 100 silicon exceeds typical variations in fiber diameter. GaAs etchants, on the other hand, are not nearly as directional and thus significant undercutting of the oxide mask occurs. Up to 12 microns or so of undercutting can be compensated by making a narrower slot in the oxide, but the slot must be wide enough to admit the fiber diameter. Therefore, the rate of undercutting must be less than about 20 percent of the vertical (i.e., 100) etch rate.

A number of GaAs etchants were tested in an attempt to find one that would be sufficiently anisotropic. Our best results were obtained with acidic hydrogen peroxide etchants. These consisted of varying concentrations of H_2SO_4:H_2O_2:H_2O, H_3PO_4:H_2O_2:H_2O, or HCl:H_2O_2:H_2O. We also tried mixtures of NH_4OH:H_2O_2:H_2O. However, after extensive experimentation with these etchants, we were lead to conclude that none of them would offer sufficient anisotropy for single-mode fiber-to-waveguide coupler vee-grooves. Our better results are shown in Figure 3-13.

Figure 3-13. Etched Vee-Grooves in GaAs. We conclude that available GaAs etches are not sufficiently anisotropic to produce vee-grooves for fiber alignment.

In contrast to the GaAs results, excellent vee-grooves can be fabricated in Si using KOH as the etchant. Figure 3-14 shows typical results obtained under a Honeywell-funded IR&D program. We conclude that fiber-to-waveguide coupling to GaAs devices is best accomplished using Si vee-groove blocks for fiber alignment. We envision two distinct variations. First, fibers could be embedded in a silicon block which would then be cut and polished for edge-to-edge coupling with a cleaved GaAs device. The second method would be to half bury cleaved fibers in stopped Si vee-grooves and then mount the Si block face-to-face with a GaAs device so that the cleaved fiber ends would butt to a cleaved edge of the GaAs device. The second method has the advantage of not requiring edge polishing of the Si block. We were unable to demonstrate either of these alternative methods within the resources of the program.

Figure 3-14. Etched Vee-Grooves in Silicon. Fabricated under a Honeywell-funded IR&D program, these precise grooves indicate the type of structure we had hoped to demonstrate in GaAs.

Another aspect of fiber-to-waveguide coupling is mode matching. In contrast to Ti:$LiNbO_3$ waveguides, our thin-film waveguides are well matched to diode lasers but poorly matched to fibers. The mode dimensions of our single mode thin-film waveguides are about 2.5 um horizontal by 1.0 um vertical. Typical single mode fibers have mode diameters of 5 to 6 um. Simple butt coupling of fiber to waveguide results in losses of 9 to 11 dB due almost entirely to the difference in mode dimensions.

There are a number of possible approaches to improving mode matching. Horizontal matching can be readily achieved by tapering the channel waveguide into a horn structure. As reported above, we were successful in showing that such tapering can be accomplished with negligible mode conversion losses. Mode matching in the vertical dimension is less easily achieved. We had originally proposed using an optical fiber in a transverse vee-groove as a cylindrical lens, overlooking the fact that transverse grooves in GaAs have dovetail profiles. A better approach is to increase the vertical mode dimension of the thin-film waveguide by reducing the thickness of the waveguiding film.

Figure 3-15 shows the dependence of mode dimension on film thickness for a symmetric SiO_2-ZnO-SiO_2 structure. Figure 3-16 depicts how film tapering could be used to achieve fiber-to-waveguide vertical mode matching. The waveguiding film thickness of 3000 A (4700 A in Al_2O_3) is selected in order to achieve low-loss single-mode operation. For a symmetric guide (one having identical cladding and buffer layers), a much thinner waveguiding film will result in a significantly increased mode dimension. A film thickness of about 100 A, equal to the waveguide ridge height, should result in a vertical mode dimension of 4 microns, about the same as the mode diameter of an optical fiber.

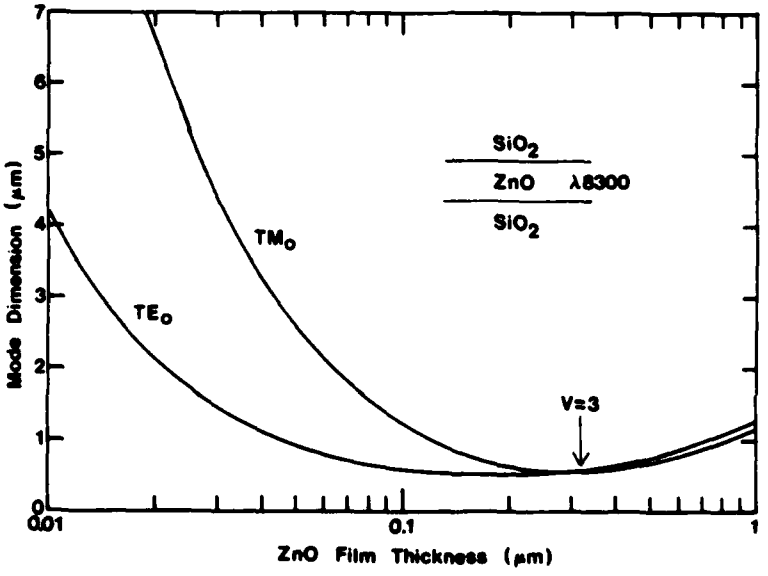

Figure 3-15. Dependence of Mode Dimension on ZnO Film Thickness. The most effective (and easiest) method of increasing the optical mode dimension is to decrease the ZnO film thickness.

An appropriately tapered structure can be produced by first depositing the 100 A ridge and then using a mechanical shadow mask to taper the subsequent planar ZnO deposition to zero in the vicinity of the vee-grooves. The exact location and rate of the tapering are not critical; a more gradual transition will reduce mode conversion losses, but a longer propagation distance at the larger mode dimension will result in

greater losses to the substrate. The tapering should have the additional benefit of reducing the effective refractive index of the waveguide, thus reducing Fresnel reflections at the junction. Overall, the coupling loss should be reduced from an initial 9-11 dB to perhaps 3 dB.

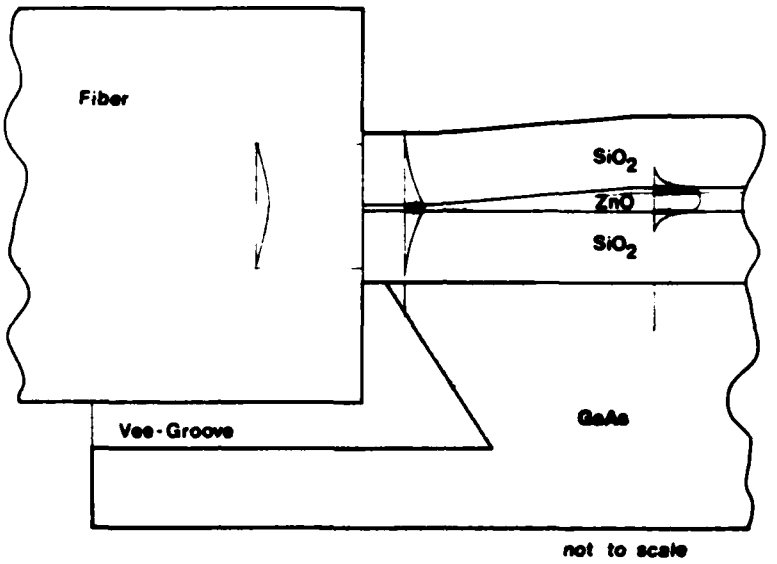

Figure 3-16. Concept for Fiber-to-Waveguide Mode Matching. The shaded areas represent the optical mode profile at three dissimilar points along the path. Tapering the ZnO film thickness enlarges the waveguide mode dimension to better match that of the fiber.

Because suitable waveguiding films were obtained so late in the program, we found ourselves unable to demonstrate our concept for vertical mode matching.

ELECTRO-OPTIC SWITCHES AND MODULATORS

Electro-optic devices are key components in many integrated optic circuits. ZnO is an electro-optic crystal with hexagonal (6 mm) symmetry. Sputtered films of ZnO are generally polycrystalline with the c-axis oriented vertically but orthogonal axes oriented randomly in the plane. Therefore, only vertical field components can contribute to a net electro-optic effect. The relevant electro-optic coefficients are r_{13} = -1.4 x 10 pm/V for TE modes and r_{33} = +2.6 x 10 pm/V for TM modes. Although parallel surface electrodes will yield vertical field components, vertical fields are more efficiently produced by placing electrodes both above and below the ZnO film. Despite the smaller r_{13} coefficient, TE mode devices are to be preferred because of the stronger attenuation of TM modes by the electrode structure.

Uncompensated ZnO films are semiconducting. An average breakdown voltage $E_{max} = 8 \times 10^6$ V/m has been reported; corresponding to a maximum electro-optically induced refractive index change of $n = -n^3 r E_{max}/2 = \pm 4 \times 10^{-5}$. For electro-optic devices requiring a $\pm$ /2 phase shift, electrical breakdown dictates a minimum device length of 5 mm, roughly twice the length of comparable $LiNbO_3$ devices. There is, however, a significant difference. The length of a $LiNbO_3$ electro-optic device is typically limited by the need for a reasonable drive voltage (50-100 V), whereas thin-film ZnO devices should operate at much lower drive voltages (8-12 V) because their vertical electrode structure typically results in a narrower electrode gap. Moreover, higher quality films are expected to exhibit higher breakdown voltages. The conductivity of ZnO can also be compensated by doping with lithium.

Because of our substitution of nonelectro-optic Al_2O_3 for ZnO, we were unable to test any electro-optic switches. We have, as reported above, fabricated several relevant waveguide structures such as Y-branches and directional couplers. It was our intent to demonstrate thin-film electro-optic switches of both the directional coupler and Mach-Zehnder types. The directional coupler switches (Figure 1-2) were designed with an electrode length of 3 mm. This is somewhat less than the calculated minimum length based on average breakdown voltage. We felt, however, that the benefits of demonstrating shorter devices outweighed the risk of not being able to fully modulate them. Since the ZnO breakdown voltage has been reported to vary from 5×10^6 to at least 20×10^6 V/m, it seemed likely that at least some of our devices would be electrically functional. The required drive signals were estimated to be in the vicinity of 20 volts.

Had we been successful in obtaining ZnO films of acceptable optical quality, our electro-optic devices would have been as short as their $LiNbO_3$ counterparts while operating at somewhat lower drive voltages.

INTEGRATED PHOTODETECTORS

Simple, efficient, and very high-speed Schottky photodiodes can be easily fabricated on semi-insulating GaAs substrates. Such a detector consists of an appropriately patterned pair of Schottky metallization contacts. Under illumination, photocarriers are generated in the diode depletion region surrounding each Schottky contact. The associated DC photocurrent increases monotonically with increasing bias voltage. Generally, in order to obtain a large area detector, the Schottky metallization has consisted of a pair of interdigitated electrodes. A disadvantage of this configuration is that a portion of the incident light is blocked by the electrodes. Moreover, a channel waveguide photodetector need not have a large area of sensitivity. We therefore developed a unique approach in which two parallel Schottky electrodes straddle the channel waveguide.

Our integrated waveguide photodetectors are shown in Figure 3-17. The electrodes extend through an opening in the SiO_2 buffer layer to form Schottky contacts to the semi-insulating GaAs substrate. Depending on

the doping concentration, a bias voltage of 20 to 50 volts can be expected to extend the diode depletion region fully across the 8-micron inter-electrode gap. As light couples from the channel waveguide to the higher index GaAs, photocarriers are generated in the inter-electrode gap. Up to the breakdown voltage of the GaAs, the photocurrent should increase monotonically with increasing bias. The measured performance of a typical working detector is shown in Figure 3-18.

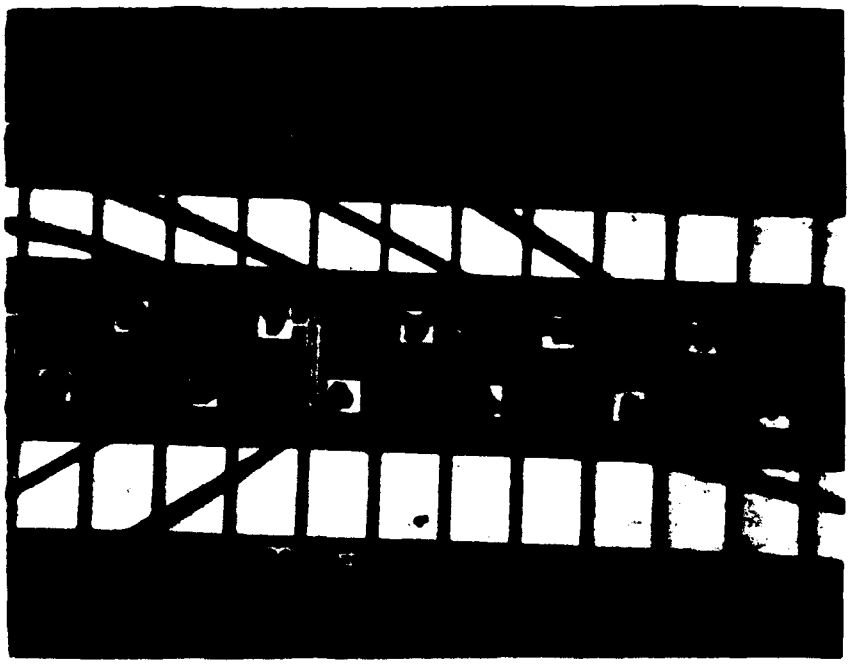

Figure 3-17. Integrated Schottky Photodetectors. Slots in the SiO_2 buffer layer allow coupling of light from the thin-film channel waveguides to the GaAs substrate. Two parallel Schottky contacts straddle each slot to form a simple but effective photodiode.

For the parallel electrode geometry, we expected virtually no absorption of light by the electrode structure. In fact, by optionally omitting the buffer layer openings, we demonstrated that we could make the detectors invisible to the optical guided waves. This proved a most useful option when testing the other waveguide devices.

The concept worked, but some of the features which allowed the photodetectors to be optional also caused their yield and performance to be poor. In particular, it was difficult to open the slots in the thick SiO_2 buffer layer and do the liftoff photolithography in a manner which

would yield good Schottky contacts. Problems included photoresist residue at the bottom of the slots and damage to the GaAs substrate by the plasma etching process. Also, the 8 micron inter-electrode gap was unnecessarily wide compared to the observed waveguide mode width of 2.6 microns.

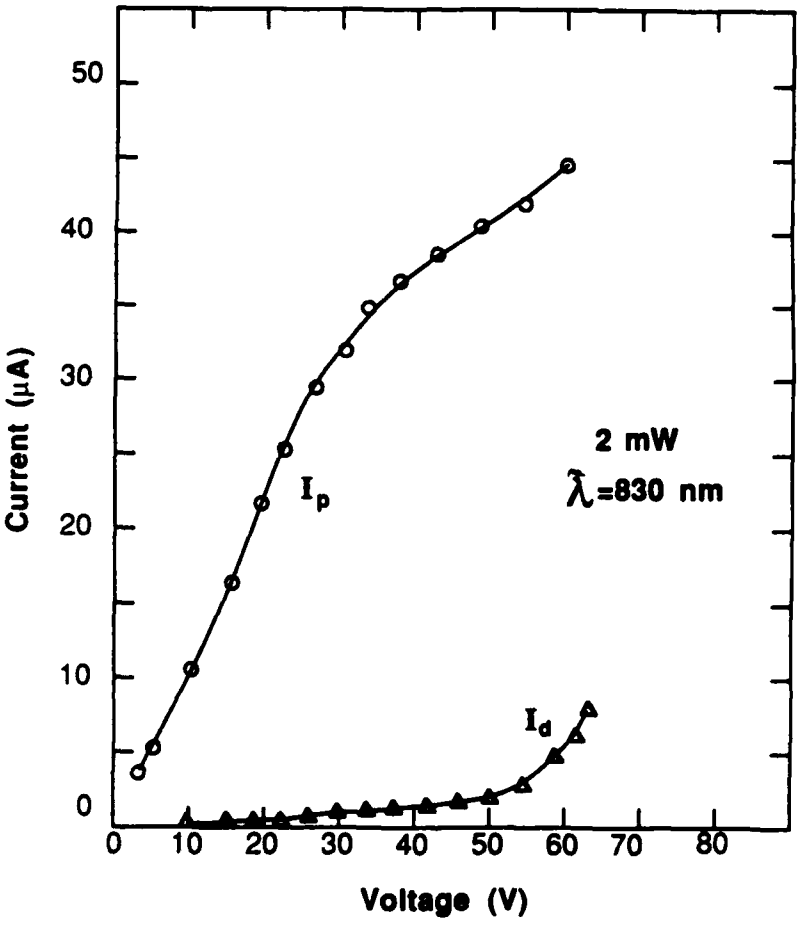

Figure 3-18. I-V Characteristics of Back-to-Back Schottky Photodetector.

We feel these channel waveguide photodetectors could be considerably improved by narrowing the inter-electrode gap to about 4 microns and completing the Schottky metallization prior to depositing the SiO_2 buffer layer. The maximum useful electrode length for an integrated waveguide photodetector is dependent on the distance required to couple light from the waveguiding film to the GaAs substrate and also on the amount of scattering or spreading occuring when the optical guided wave encounters the buffer layer opening. Excessive electrode length (or width) will result in larger dark current and capacitance. We fabricated detectors with buffer layer openings varying in length from 50 to 300 microns. However, the erratic quality of the Schottky contacts prevented us from making meaningful comparisons.

SUMMARY OF ACCOMPLISHMENTS

The overall objective of the Thin-Film Optoelectronic Circuits Research Program has been to identify and investigate IC-compatible fabrication processes for thin-film optoelectronic circuits of ZnO on GaAs. By substituting ion-beam sputtered Al_2O_3 for ZnO, we achieved significant results on a number of tasks despite a continued lack of suitable quality ZnO films. The technology which we have developed and demonstrated will contribute to the monolithic integration of optical components with mainstream GaAs and Si microelectronics. Our major accomplishments are as follows:

- Established the suitability of plasma deposited SiO_2 as a low index buffer layer for thin-film waveguide structures fabricated on GaAs.
- Developed and demonstrated an innovative and versatile ridge deposition technique for fabricating thin-film channel waveguides having overall optical attenuation of less than 1 dB/cm with minimal scatter due to sidewall roughness.
- Fabricated and tested a variety of low optical attenuation, single mode, channel waveguide bends, tapers, Y-couplers, directional couplers, and crossovers.
- Proposed two fiber-to-waveguide coupling techniques utilizing silicon vee-grooves and demonstrated fiber-to-fiber alignment with coupling efficiencies of better than 80 percent. Developed a method of permanently mounting fibers in vee-grooves.
- Designed efficient thin-film ZnO electro-optic switches which we expect could operate at lower drive voltages than $LiNbO_3$ switches of comparable length.
- Developed and successfully demonstrated a novel concept for monolithically integrated channel waveguide Schottky photodetectors.
- Developed and extensively refined an IC-compatible fabrication process for thin-film optoelectronic circuits on GaAs.
- Designed and attempted fabrication of a thin-film optoelectronic circuit which included 1 x 4 and 2 x 2 optical crossbar networks, Mach-Zehnder interferometric waveguide modulators, and integrated GaAs photodetectors.

Section IV
DIRECTIONS FOR FUTURE RESEARCH

The Thin-Film Optoelectronic Circuits Research Program has successfully developed and demonstrated IC-compatible fabrication of several thin-film integrated optic devices on GaAs substrates. When compared to AlGaAs devices on GaAs, our thin-film waveguide devices exhibit the advantages of lower attenuation loss and greater ease of fabrication. Although we have not explicitly demonstrated the integration of optical and electronic components on a common substrate, the IC compatibility of our fabrication process makes the feasibility of monolithic integration a virtual certainty.

The first task of further research is to complete the demonstration of electro-optic switching in thin-film channel waveguides. Although we were unable to obtain ZnO films of sufficient optical quality, we did demonstrate the relevant waveguide structures and fabrication procedures. As several research groups have already shown, a modest materials program using a dedicated r.f. sputtering system can produce ZnO thin films of high optical quality.

The logical next step following a successful demonstration of electro-optic switching is the integration of thin-film waveguide devices with an AlGaAs diode laser. The ability to monolithically integrate a laser has formed Honeywell's primary justification for fabricating thin-film ZnO optical circuits on substrates of GaAs rather than silicon. As demonstrated in our Fiber Optic Gyro program (IR&D), silicon substrates have the advantages of a high quality native oxide and superior anisotropic etching properties. The key technical challenge to monolithically integrating an AlGaAs laser with ZnO (or any other) waveguide devices involves developing an on-chip mirror that will facilitate coupling of the laser to an on-chip thin-film waveguide. Two possibilities include ion-etched facets, and grating mirrors such as those used on distributed Bragg reflector (DBR) lasers; the former promises greater ease of coupling to thin-film waveguides.

A third area meriting further investigation is the incorporation of acousto-optic devices with thin-film optoelectronic circuits. Whereas GaAs itself has negligible piezoelectric coefficients, oriented ZnO thin films exhibit a moderately strong piezoelectric effect which can be used to launch surface acoustic waves (SAWs) by means of interdigitated electrode transducers. Optoelectronic circuits relying solely on channel waveguides and electro-optic switches offer high-speed operation, but they have been of rather limited complexity because of the long electrode length (millimeters) needed to obtain a sufficient interaction. By contrast, SAW devices, using planar ZnO waveguides, can take advantage of the massive parallelism inherent in optics. Possible devices include the RF spectrum analyzer and the synthetic aperture radar (SAR) processor.

Section V
APPENDIX

PROGRAM ORGANIZATION

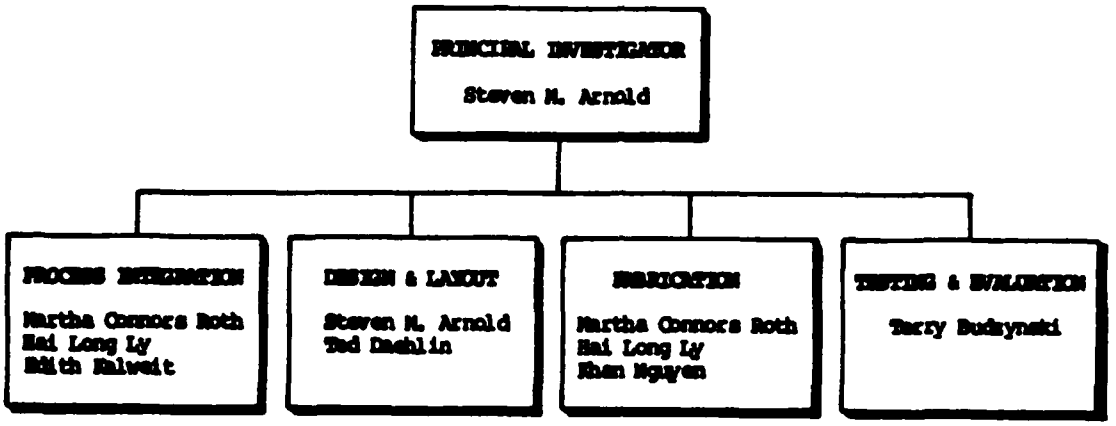

Figure 5-1. Program Organization.

PUBLICATIONS

The following patents and publications are anticipated to result from the Thin-Film Optoelectronic Circuits Research Program:

- o Channel Waveguide Schottky Photodiode. A patent disclosure describing our monolithically integrable back-to-back Schottky diode photodetector.

- o Low-Loss Thin-Film Ridge Waveguides on GaAs. A journal article describing our Al_2O_3 ridge waveguide and integrated photodetector fabrication processes and reporting channel attenuation losses of 0.9 dB/cm. In preparation for submission to Applied Optics.

ACKNOWLEDGEMENT

The Principal Investigator would like to thank Dr. Charles T. Sullivan for his assistance in completing this report.

PHASE I MASK SET

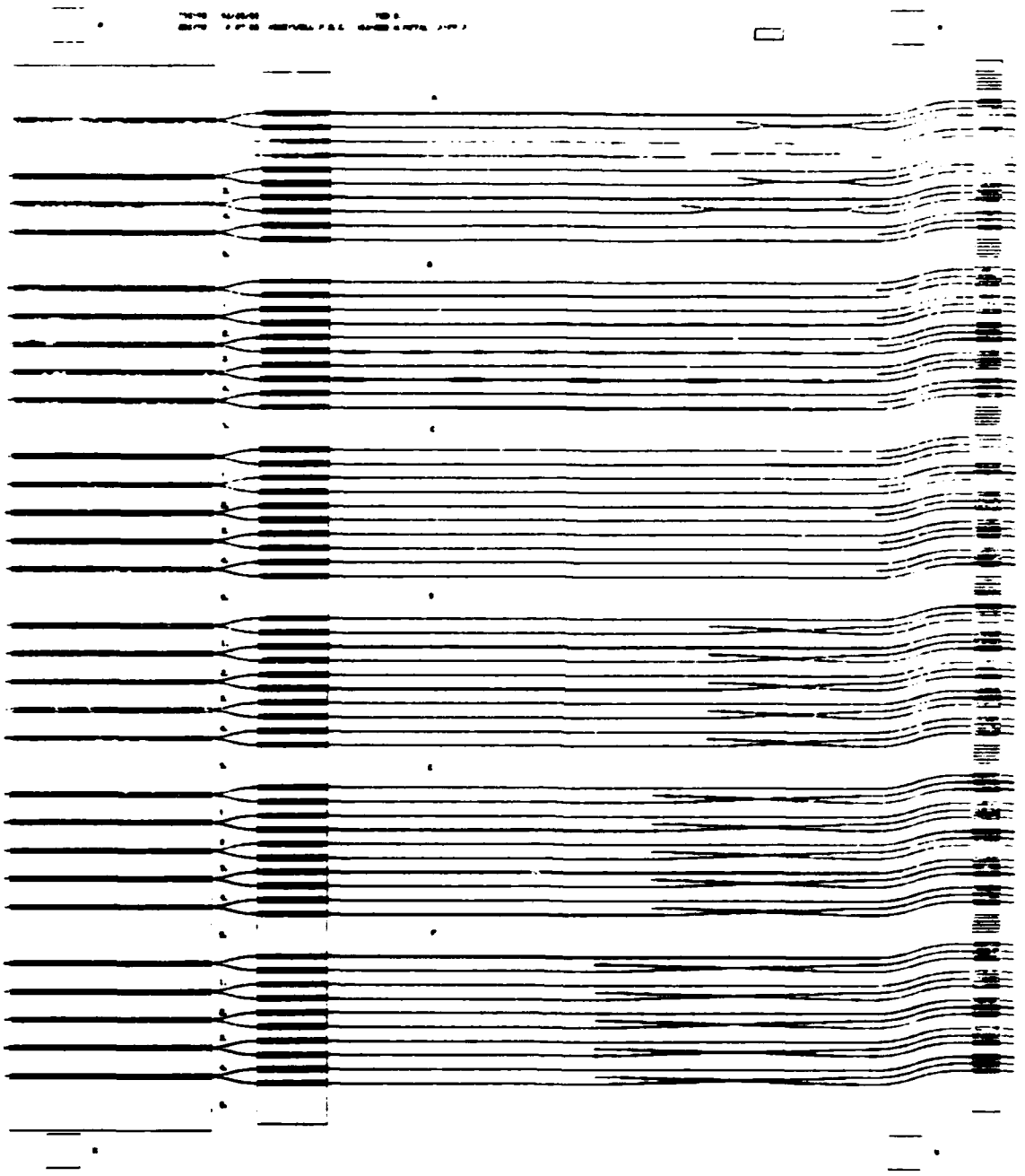

Figure 5-2. Computer Plot of Phase I Mask Set. The metal lization pattern (rectangles) on the first mask level helped in locating and identifying the channel waveguide structures while also absorbing unwanted planar waveguide modes.

PHASE II FABRICATION PROCESS

STEPS	PROCEDURE	DESCRIPTION	DATE/ INIT	PARAMETERS	COMMENTS
1.0		CLEAN AND ETCH			
1.1	WC-15	Solvent clean		Ultrasound PRS-1000 88 C.5 min 9 quick dumps IPA 5 min DI water 5 min 2 quick dumps Rinse/dry	
1.2	PR-04	High pressure scrub		Program 1. no bake	
1.3	WC-34	Wet chemical etch		HCl 60 sec 9 quick dumps 10:1:1 H2SO4:H2O2: DI H2O 2 min 9 quick dumps	
2.0		BUFFER AND DETECTOR APERTURES			
2.1	WC-32	Pre-clean Immediately before deposition		10:1 H2O:NH4OH 90 sec.9 quick dumps solvent processor#1	
2.2	D-RF-03	Plasma oxide dep.		1.3 microns	
2.3	PR-04	Photolithography Mask 5068-A-10 Detector apertures		Develop cycle #4 bake 60 sec. HMDS. #4 coat PR. 4000RPM 40 sec bake.3 sec expose. dev #1. descum LFE 3 min	
2.4	DP-11	Plasma etch silicon oxide ETCH TIME:		Lam etcher 800-900A/min in 5 min increments;250W 800mTorr. 52cm gap 27sccm CHF3.173sccm C2F6 (Freon 23&116)	
2.5	DP-07	Plasma strip 5 min		300 Watts.750 mTorr	
2.6	WC-45	PRS-1000 strip		85 C soak dump rinse 3x Solvent processor#6	
2.7	DP-27	Descum 6 min		300 Watts.200 mTorr	
3.0		LOWER METALLIZATION			
3.1	PR-04	Photolithography Mask 5068-A-20 TWO LAYER RESIST		Develop cycle #4 60 sec bake. HMDS. coat PMMA#6.5000RPM bake 170 C. 70 sec coat PR #1. 5000RPM expose 2sec.bake #1 develop #1. bake #1 descum 9 min. 0.2T UV expose. develop PMMA	
3.2	WC-32	Pre-clean Immediately before deposition		10:1 H2O:NH4OH 15 sec. rinse/dry	
3.3	M-8	Sputter deposition Schottky metal		Cr 250 A	
3.4	WC-37	Liftoff		IPA soak 20 min PRS-1000 88 C Ultrasound 9 dumps Solvent processor#1	
3.5	DP-27	Plasma descum 3 min		300 Watts.200 mTorr	
3.6	WC-32	Pre-clean Immediately before deposition		10:1 H2O:NH4OH 90 sec.9 quick dumps solvent processor#1	
3.7	D-RF-03	Plasma oxide dep.		1000 A	
4.0		DETECTOR TEST			
4.1		Test			
4.2	DP-27	Descum 6 min		300 Watts.200 mTorr	

5.0		CHANNEL WAVEGUIDES			
5.1	PR-04	Photolithography Mask 5065-A-30 LINEWIDTH? TWO LAYER RESIST		Develop cycle #4 bake 60 sec, HMDS. Coat PMMA, 5000RPM bake 170 C coat PR #1, 5000RPM expose 2sec.bake #1 develop #1, bake #1 descum 9 min, 0.2T UV expose, develop PMMA	
5.2	WC-32	Pre-clean Immediately before deposition		10:1 H2O:NH4OH 15 sec, rinse/dry	
5.3		Ion beam deposit waveguide ridge		FILM TYPE? THICKNESS? PARAMETERS?	
5.4	WC-37	Liftoff		IPA soak 20 min PRS-1000 85 C Ultrasound 9 dumps	
5.5	DP-27	Plasma descum 3 min		300 Watts, 200mTorr	
5.6	WC-32	Pre-clean Immediately before deposition		10:1 H2O:NH4OH 15 sec, rinse/dry	
5.7		Ion beam deposit planar film		FILM TYPE? THICKNESS? PARAMETERS?	
6.0		PRISM COUPLE MEASUREMENT			
6.1		Measure			
6.2	DP-27	Descum 6 min		300 Watts,200 mTorr	
7.0		WAVEGUIDE FILM ETCH			
7.1	PR-04	Photolithography Mask 5065-A-60		SLIGHTLY OVEREXPOSE	
7.2		Etch waveguide film			
7.3	WC-48	PRS-1000 strip		85 C soak dump rinse 9x	
7.4	DP-27	Plasma descum 3 min		300 Watts,200 mTorr	
8.0		UPPER METALLIZATION			
8.1	D-RF-03	Plasma oxide		1000 A	
8.2	PR-04	Photolithography Mask 5065-A-50 TWO LEVEL RESIST		Develop cycle #4 60 sec bake, HMDS, coat PMMA6,5000RPM bake 170 C coat PR #1, 5000RPM expose 2sec.bake #1 develop #1, bake #1 descum 9 min, 0.2T UV expose, develop PMMA	
8.3	WC-32	Pre-clean Immediately before deposition		10:1 H2O:NH4OH 15 sec, rinse/dry	
8.4	M-E	E-Beam deposition		Ti 100 A, Au 1200 A Pt 150 A	
8.5	WC-37	Liftoff		IPA soak 20 min PRS-1000 85 C Ultrasound 9 dumps	
8.6	DP-07	Plasma strip 10 min		300 Watts 750 mTorr	
9.0		CONTACT PADS			
9.1	PR-04	Photolithography Mask 5065-A-40		Develop cycle #4 60 sec bake, HMDS, coat PR #4, 5000RPM bake #1, 4 sec exp bake #1, develop #1 bake #1	
9.2	DP-27	Descum 4 min		300 Watts,200 mTorr	
9.3	DP-11	Plasma etch 1000 A silicon oxide		Lam etcher 800-900A/min in 5 min increments:250W 900mTorr, .82cm gap 27sccm CHF3,17Sccm C2F6 (Freon 23&116)	
9.4		Etch waveguide film			

9.5	WC-45	PRS-1000 strip		85 C soak dump rinse 9x Solvent processored	
9.6	DP-27	Descum 6 min		300 Watts,200 mTorr	
9.7	PR-04	Photolithography Mask 5065-A-40		Develop cycle #4 60 sec bake. HMDS. coat PR #4, 5000RPM bake #1, 4 sec exp bake #1, develop #1 bake #1	
9.8	DP-11	Plasma etch 1000 A silicon oxide		Lam etcher 800-900A/min in 5 min increments;250W 800mTorr, .52cm gap 27sccm CHF3,173sccm C2F6 (Freon 236116)	
9.9		Pre-deposition treatment			
9.10	M-E	E-Beam deposition		Ti 500 A,Au 3000 A Pt 150 A	
9.11	WC-37	Liftoff		IPA soak 20 min PRS-1000 85 C Ultrasound dump rinse 9x	
9.12	DP-07	Plasma strip 10 min		300 Watts 750 mTorr	
10.0		PASSIVATION			
10.1	WC-32	Pre-clean Immediately before deposition		10:1 [illegible] 60 sec. rinse/dry	
10.2	D-[illegible]-03	Plasma oxide dep.		1.0 micron	
11.0		VIA-GROOVES			
11.1	PR-04	Photolithography Mask 5065-A-60			
11.2	DP-11	Plasma etch silicon oxide		Lam etcher 800-900A/min in 5 min increments;250W 800mTorr, .52cm gap 27sccm CHF3,173sccm C2F6 (Freon 236116)	
11.3	WC-	Anisotropic GaAs etch			
11.4		Photoresist removal		Solvent proc. #3 asher strip 6 min	
12.0		CONTACT PADS			
12.1		VIA-fill photolith		fill v-grooves	
12.2	PR-04	Photolithography Mask 5065-A-60		Develop cycle #4 60 sec bake. HMDS. coat PR #4, 5000RPM bake #2, 4 sec exp bake #1, develop #1 bake #1	
12.3	DP-27	Descum 4 min		300 Watts,200 mTorr	
12.4	DP-11	Plasma etch silicon oxide		Lam etcher 800-900A/min in 5 min increments;250W 800mTorr, .52cm gap 27sccm CHF3,173sccm C2F6 (Freon 236116)	
12.5		Post plasma skin and photoresist removal		Plasma ash 5 min plasma strip 15 min	

PHASE II MASK SET

The next several figures are CALMA plots of the six level, Phase II mask set. This e-beam generated mask set has been shared equally by the Thin-Film Optoelectronic Circuits Research Program (bottom half, ZnO on GaAs) and the Honeywell-funded Fiber Optic Gyro Program (top half, ZnO on Si). The decision to share the mask set between two programs was based on a desire to maximize the number of mask design iterations affordable within each program's budget. Overall chip dimensions are 30 mm by 21 mm, of which equal 30 mm by 9 mm areas are devoted to each program and the remaining space (three areas, each 30 mm by 1 mm) contains alignment marks and test patterns. Vee-grooves on 200 micron centers occupy the last 5 mm at each end of the chip, leaving each program with an area of 20 mm by 9 mm for waveguides and active devices.

Figure 5-3. Computer Plots of Phase II Mask Set. Following an all-layers plot, plots of individual mask levels are presented in the order of their occurrence in the fabrication process.

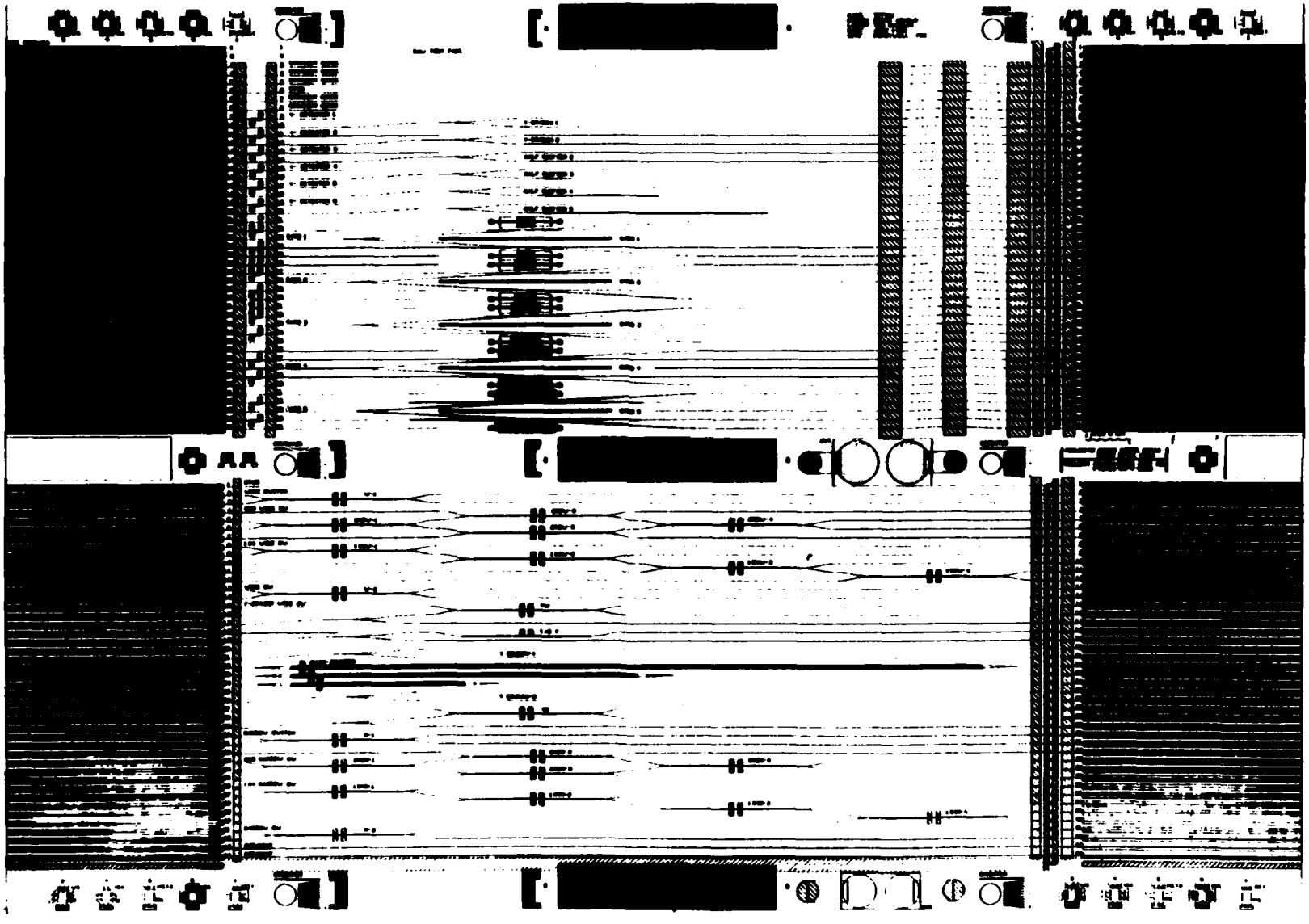

All Layers

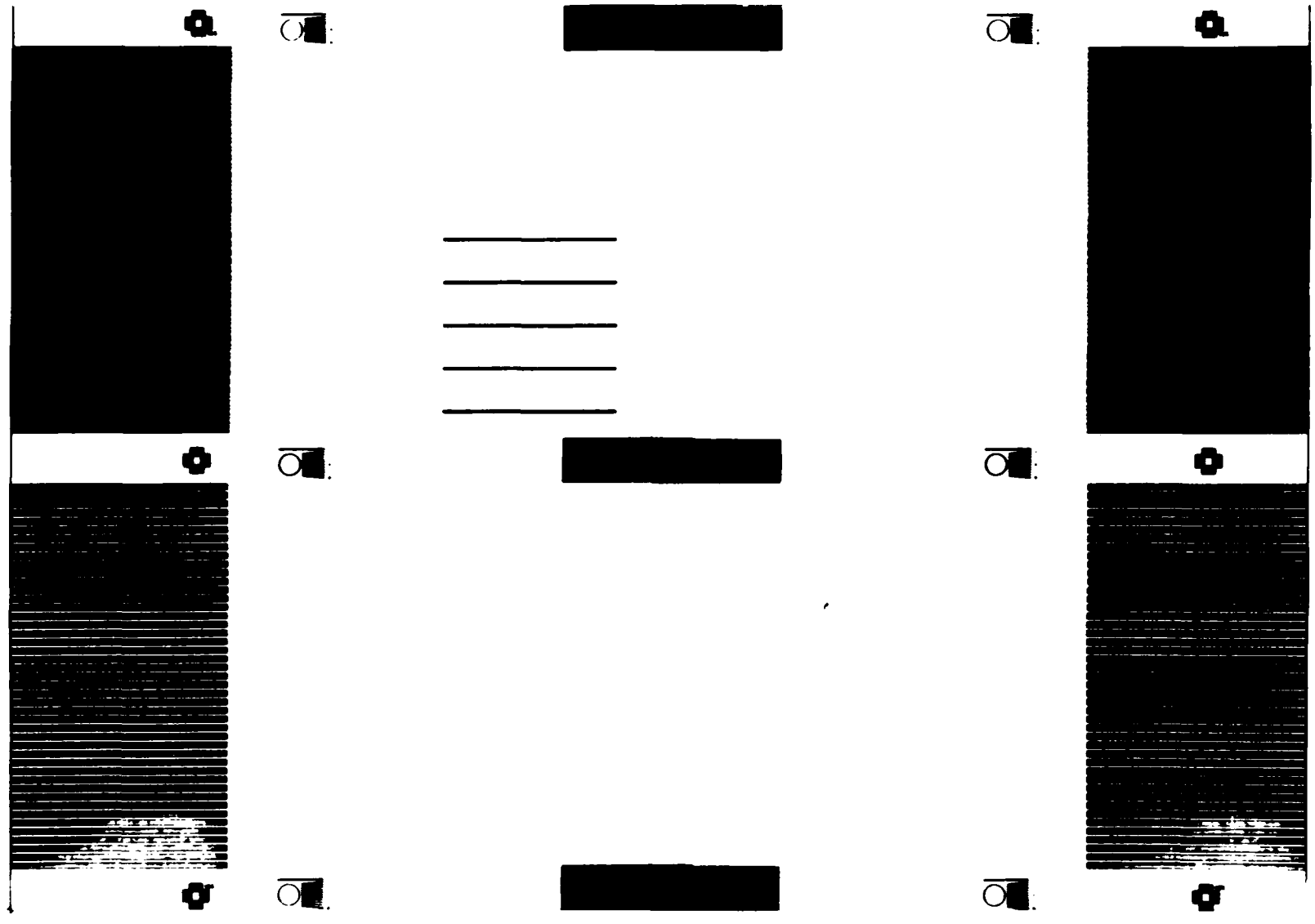

Layer 6 Vee-Grooves

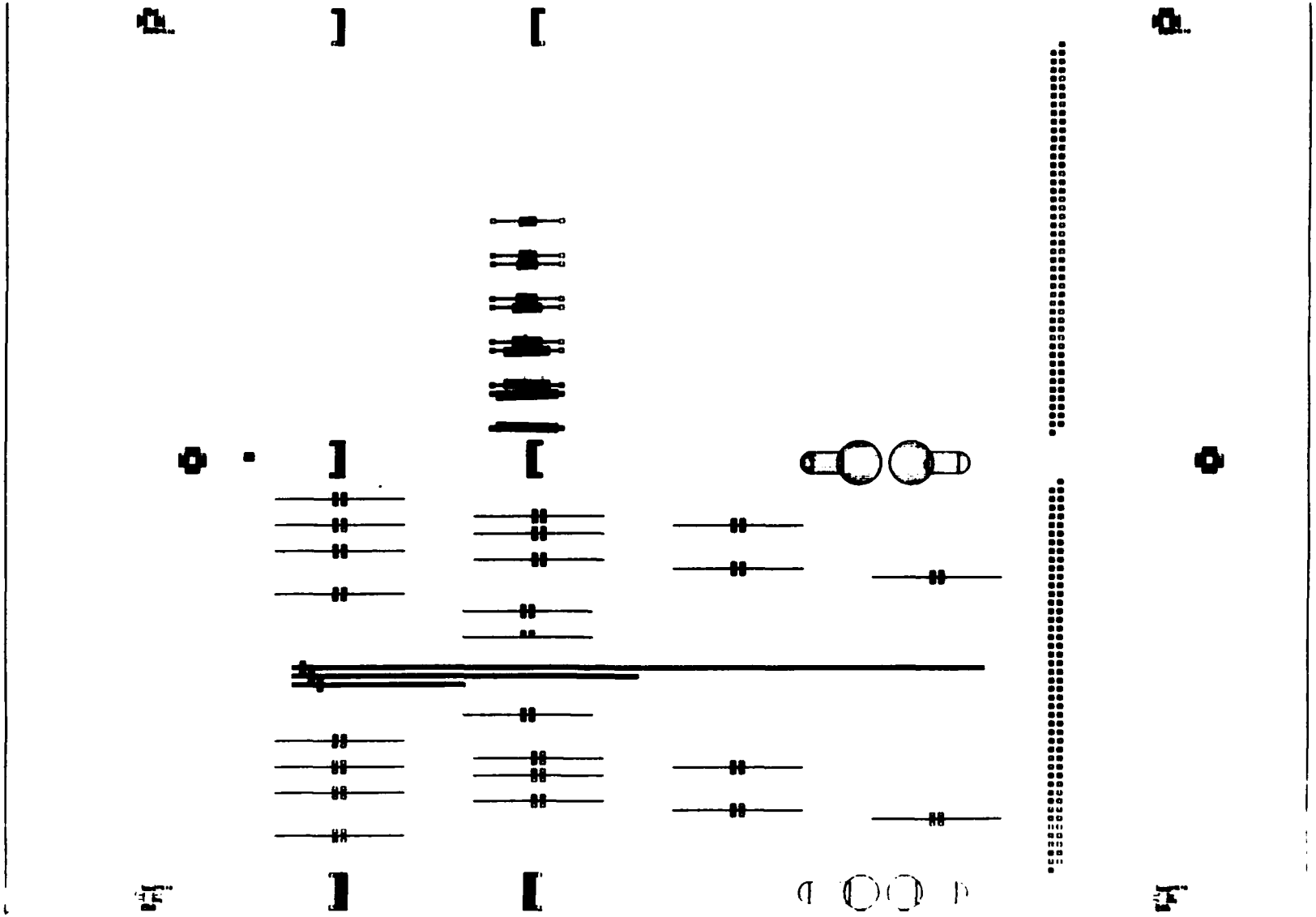

Layer 5 Upper Metalization

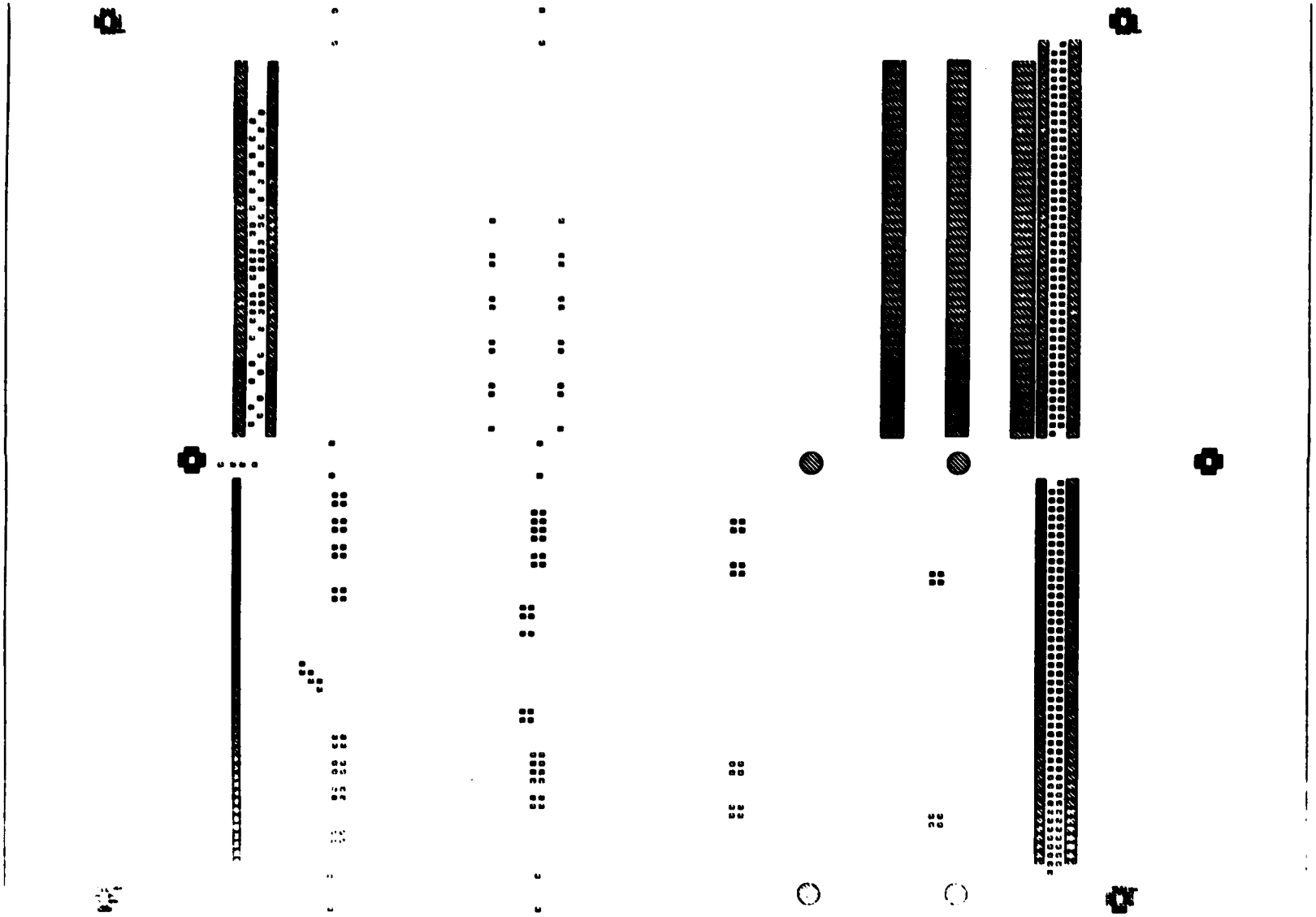

Layer 4 Contact Pads

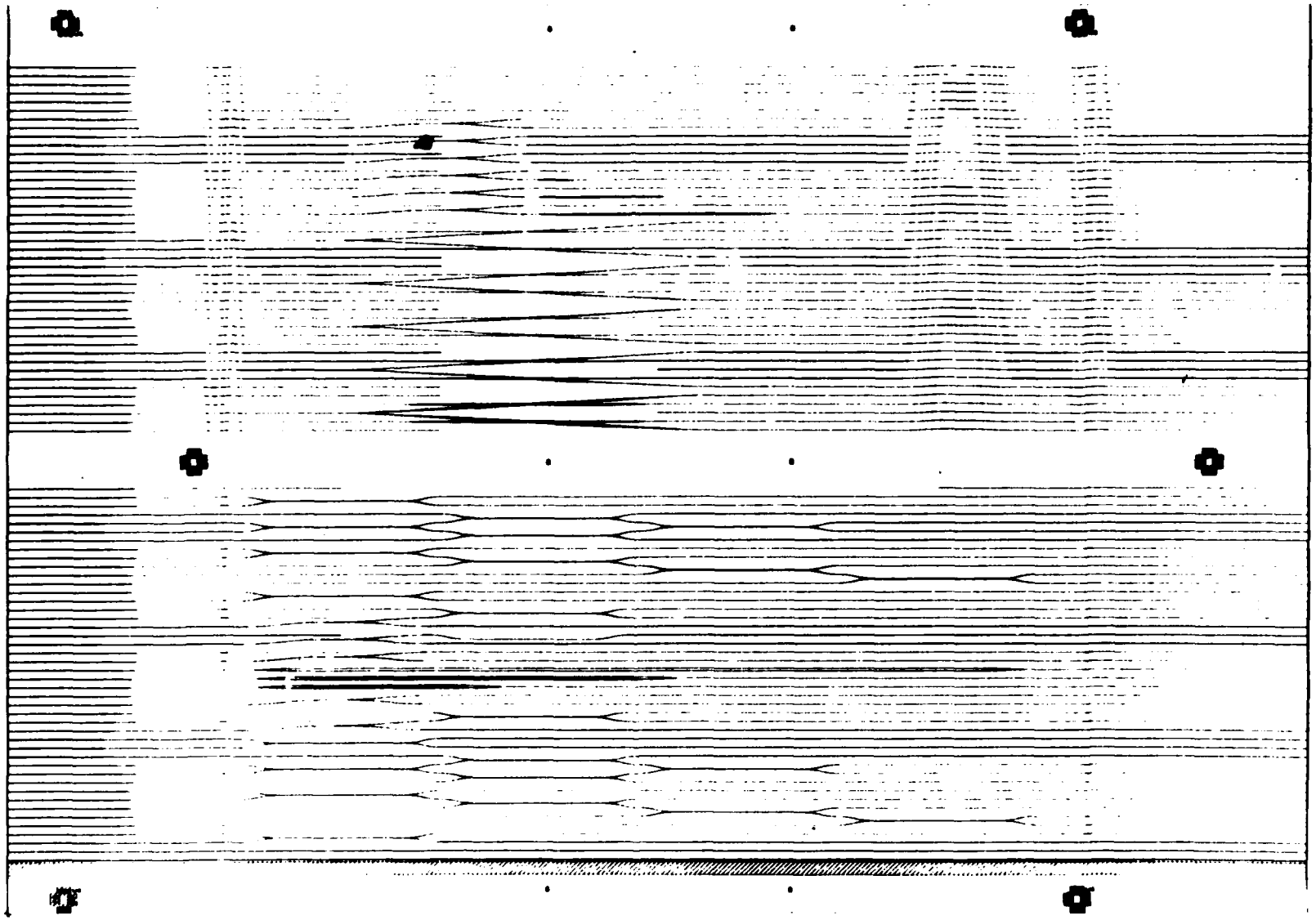

Layer 3 Waveguides

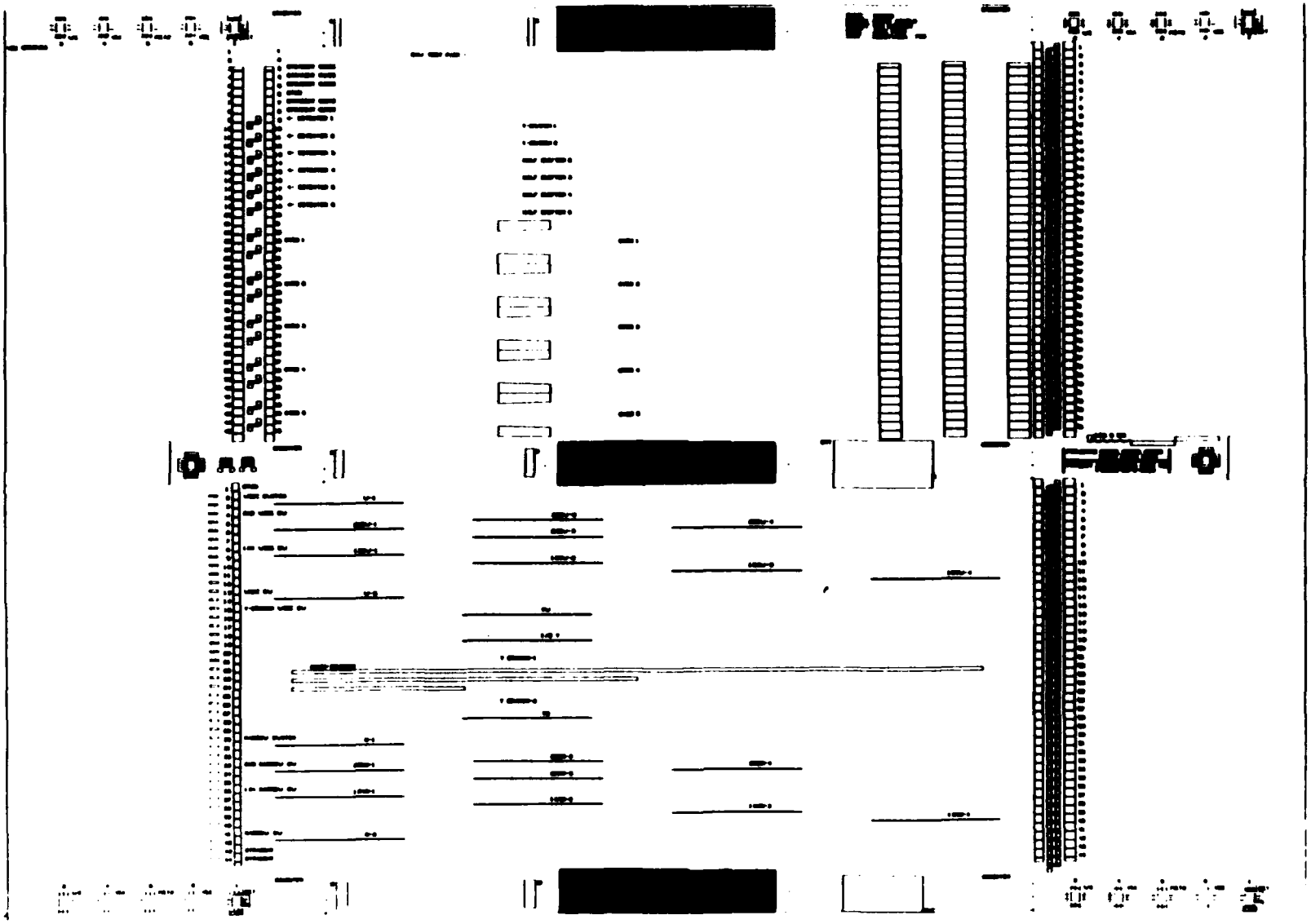

Layer 2 Lower Metalization

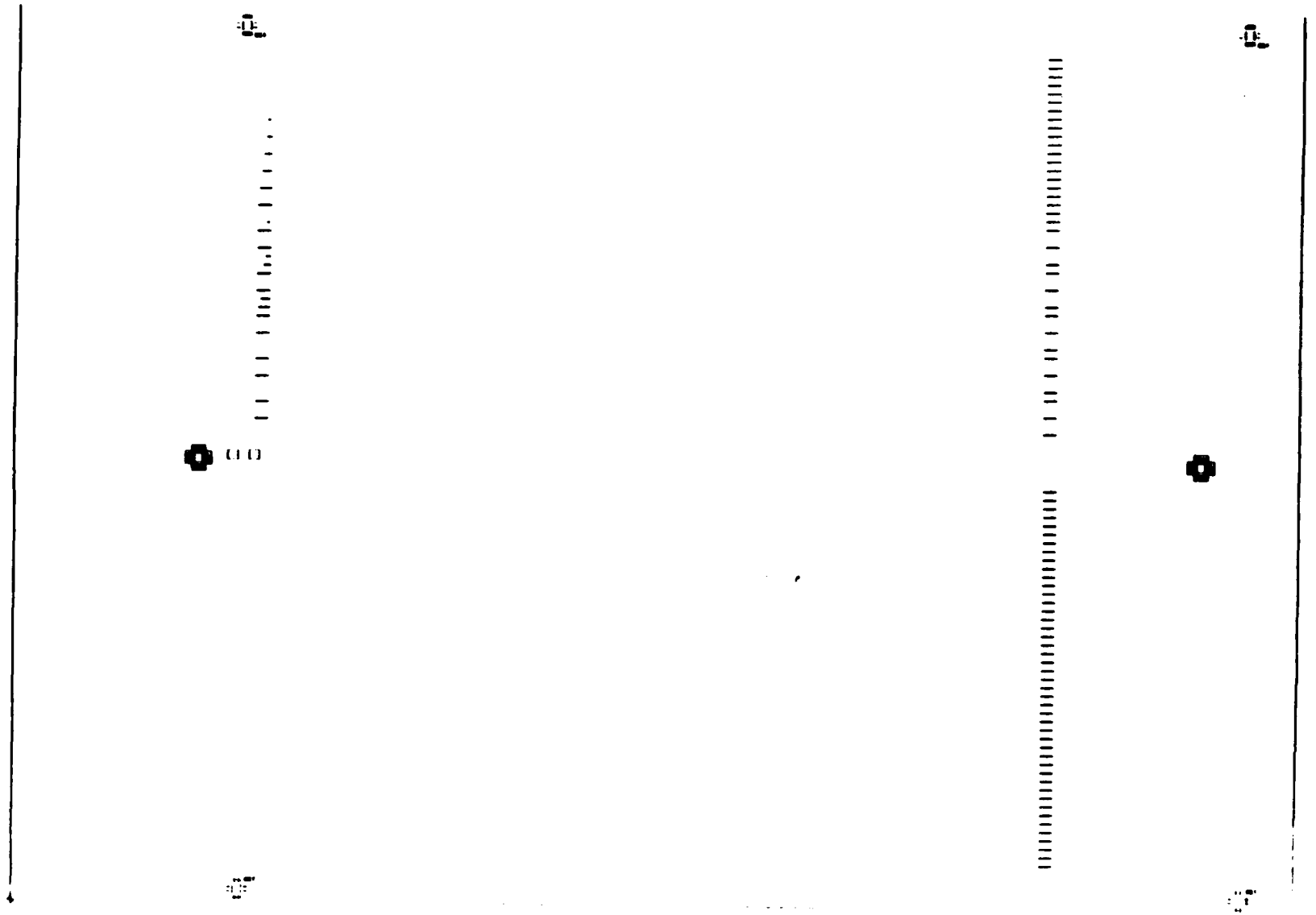

Layer 1 Detector Apertures

END

7-87

DTIC